Study of Integer Quantum Hall coupled Edge states in Monolayer and Bilayer Graphene

A Thesis

submitted to
Indian Institute of Science Education and Research Pune
in partial fulfillment of the requirements for the
BS-MS Dual Degree Programme

by

Manoj M Hegde

Indian Institute of Science Education and Research Pune
Dr. Homi Bhabha Road,
Pashan, Pune 411008, INDIA.

May, 2019

Supervisor: Dr. Sreejith. G.J

Certificate

This is to certify that this dissertation entitled Study of Integer Quantum Hall coupled Edge states in Monolayer and Bilayer Graphenetowards the partial fulfilment of the BS-MS dual degree programme at the Indian Institute of Science Education and Research, Pune represents study/work carried out by Manoj M Hegdeat Indian Institute of Science Education and Research under the supervision of Dr. Sreejith. G.J, Assistant Professor, Department of Physics, during the academic year 2018-2019.

Dr. Sreejith. G.J

Committee:

Dr. Sreejith. G.J

Dr. Arun P. Thalapillil

This thesis is dedicated to my parents

Declaration

I hereby declare that the matter embodied in the report entitled Study of Integer Quantum Hall coupled Edge states in Monolayer and Bilayer Graphene are the results of the work carried out by me at the Department of Physics, Indian Institute of Science Education and Research, Pune, under the supervision of Dr. Sreejith. G.J and the same has not been submitted elsewhere for any other degree.

Manoj M Hegde

Acknowledgments

This thesis could not have been possible without the help and support I received from many people. I am grateful to all of them.I thank my project supervisor Dr. Sreejith.G.J who motivated me to pursue the topic and explained even the minute details with great clarity and has helped me in every step of the project. I also thank Dr. Arun M. Thalapillil with whom I had many fruitful discussions. I also thank my friends who shared their knowledge and insights with me. Finally, I thank my family who have supported me in all my endeavours.

Abstract

Quantum Hall states in 2D materials are characterised by robust edge states which reflect some bulk topological order through Bulk-Edge correspondence. It is of interest to realize complex states that emerge by coupling of Quantum Hall systems. Disorder plays a critical role in the stabilization of Quantum Hall states [8]. Presence of impurities and scattering due to impurities are very important for the studies of transport properties and Quantum Hall effect experiments as they influence the conductivity, magnetic properties etc. In addition, the structure of the quantum states (more precisely, the nature of the correlations) around the disorder reveals details of the topological order contained in the system[22][23].

A Quantum Hall edge state, with it's chiral edge mode is a 1D system. In case of bilayer graphene, there is a possibility of creating edge modes that are helical, robust and with suppressed back scattering with integer and fractional statistics[21].

Due to the fact that density of states vanish at the dirac points for graphene, resulting in an absence of screening, the disorders become quite important in determining transport properties. We add a single local impurity that can couple two edge modes and provide strong short range scattering. We also change chemical potential(in case of Bilayer),tune the interlayer coupling, and study it's effects on the energy spectrum in the Hofstadter regime. By threading a magnetic flux adiabatically, spectral flow of edge states and band structures are studied. Through this work, we have identified the numerical quantities and tools that are tractable through which the physics of coupled edge theory can be studied.

Contents

Chapter 1

Introduction

Classical Hall effect was discovered in 1879 by Edwin Hall. This is the phenomenon of production of a voltage difference transverse to the applied electric filed in electrical conductors when a perpendicular magnetic field is applied. The presence of perpendicular magnetic field exerts Lorentz force on charge carriers which causes charges of one type to build up on one side of the material and the charges of other type to build up on the other side creating a potential difference. This potential difference is perpendicular to the applied electric field and a current flow as a result is noticed when an electrical connection is established. Since Hall effect discovery, many more exotic types of Hall effects have also been found out like Quantum Hall effects, spin Hall effects, Anomalous Hall effect etc. Fractional quantum hall effect is one of the only two experimentally realised examples for the macroscopic manifestation of quantum entanglement the other one being superconductivity.

The topological concept of Bulk-Edge correspondence of bulk properties influencing the edge plays an important role in our analysis of edge modes and finding of Hall conductance. In our case, the quantity we will be interested is the electrical conductivity in the direction perpendicular to applied electric field.

Graphene is a fascinating material from theoretical and technological point of view. Even though graphene, in it's pristine form has very high mechanical strength and mobility, it's practical uses are limited because of the zero bandgap and low carrier density along with relative chemical inertness[2].In order to overcome these effects, it becomes imperative to control and study disorders in graphene which can tune band gaps and increase carrier density

etc. Disorder and chiral carrier dynamics plays a critical role in explaining the peculiar quantum hall effect exhibited by graphene. Recent discoveries have put much interest on the superconductor coupled Quantum Hall states in graphene as a promising candidate for realizing efficient quantum computation. In this thesis we study the problem of Integer Quantum Hall edge modes in graphene in presence of disorder numerically in the Hofstadter regime. The IQHE edge modes are studied because the case of FQHE which involves finite density of electrons has a hilbert space which is very large. The hofstadter regime is chosen as in the opposite regime of continuum model(low energy), the magnetic flux through each plaquette is very small and to obtain a magnetic unit cell, we need to take a large number of unit cells. Analytical calculations most often include a perturbative approach. If we wish to explore the non perturbative effects, we have to look for numerical approaches.

Due to the chiral nature of edge modes in graphene under perpendicular magnetic field, they are robust in the sense that chirality forbids backscattering and even in presence of many types of disorders which we explore in the thesis, the edge modes do not get localized and they continue to propagate over long distances. These edge modes in the Quantum Hall regime for both monolayer and bilayer graphene are part of our study. We ask questions as to how robust are the IQHE edge modes in graphene by varying the scattering strength, changing random diagonal impurities, direction and magnitude of Magnetic field and chemical potential. These and many other parameters, give a rich playground to study graphene edge properties. Bilayer graphene offers even more options to explore by coupling two layers in different ways like A-A coupling, A-B coupling, B-B coupling.The possibility of coupling co-propagating modes and counter propagating modes is intriguing and already being investigated actively to realize 1D helical edge states.

In the case of GaAs, relevant disorder is a local potential on the site that can trap a quasi hole or quasi particle. In case of spin unpolarized states, one can also consider local impurities that can add an additional Zeeman pinning down spin textures, spin flip excitations etc.

In the case of graphene, there are further possibilities; one can consider impurities that locally couple to the spin or valley degree of freedom or a combination of both. In the case of bilayer QH states, there is a possibility of a local disorder that scatters electron between layers. The spin-layer-valley or spin-layer-sublattice space provides a large phase space to explore nature of impurities and edge modes.

In this project is to understand the effects of local impurities on integer quantum hall edge

states and single particle eigenstates in the Hofstadter regime and to study the robustness of edge modes under various types of couplings in monolayer and bilayer graphene along with numerical quantities that show the relevant physics with the intention to later study the same problem in continuum limit and intercating regime.

Analysis of Fractional Quantum Hall edge states is not carried out in this project. As it is a problem of interacting system whose hilbert space is large. Numerical study of Continuum model of graphene requires significant computational capacity and time because of the requirement of a large number of unit cells that are needed to form a magnetic unit cell. Both computational capacity and time were constraints for the duration of project. Spin degree of freedom gives additional effects like Zeeman splitting, spin quantum Hall states etc. We shall include these in the future works.

Preliminaries

The Quantum Hall effect is observed in two dimensional materials under low temperatures and strong magnetic fields. In this case, the Hall conductance becomes discrete and takes quantised values as the electron density is varied.The quantised values are given by integer multiples of $\frac{e^2}{h}$ to the precision of 10^{-9}. One reason to use graphene in experiments for quantum Hall effects is because it can exhibit QHE at relatively high temperatures and does not require extremely pure samples. graphene also exhibits a peculiar quantisation for conductivity with

$$\sigma_{IQHE} = (n + \frac{1}{2})\frac{4e^2}{h} \tag{1.1}$$

unlike conventional 2D materials. Graphene also exhibits $SU(4)$ quantum hall ferromagnetism in the interaction regime[4] due to the presence of valley degrees of freedom in addition to spin degrees of freedom.

Due to relativistic particles like linear dispersion, graphene exhibits relativistic landau levels and has half integer quantum hall effect. Fractional Quantum Hall effect(FQHE) occurs due to electron- electron interactions. It is explained by the theory of composite fermions and quasi particles called anyons that behave like electrons but are fractionally charged.

Bilayer graphene is actively being studied as it is one of the only few 2D-materials that can exhibit the property of tunable bandgap. In most materials, the band gaps are fixed but in bilayer graphene which in pristine form is zero gap semi metal, we can tune the bandgap

which is very exciting feature as it provides great flexibility for producing nanoelectronic devices. Twisted bilayer graphene superlattices at a "magic" twist angle of 1.1^0 has been found to be superconducting. This behaviour was initially thought to be an indication of Mott insulator later careful examination attributed this room temperature superconducting phase as emerging out of wigner crystal which hadn't been observed though it was first predicted by Wigner in 1930's. Exotic electronic states like the Fractional Quantum Hall states have also been observed in bilayer graphene.

In a strong magnetic field, the gap between landau levels are so large that we can consider the electrons to be confined to lowest landau level. With this insight, the d dimensional problem can be mapped to a $(d-2)$ dimensional ϕ^4 theory.

Inverse Participation Ratio(IPR) The IPR is a measure of the amount of localization of a wavefunction. It is defined as the inverse of the average of absolute value of fourth power of wavefunction. It is a type of scaling relation that distinguishes the edge states and bulk states. A bulk state is by definition spread everywhere in the bulk but we also know that wavefunctions are normalized. In case of graphene, this means, for bulk states, the normalization condition is:

$$\sum_{sites} |\Psi_{sites}|^2 \times Area = 1 \tag{1.2}$$

The above equation means that the probability density of a bulk state wavefunction at sites on the bulk scales as $\frac{1}{Area} \approx \frac{1}{L^2}$. So the IPR which is the inverse of the sum of fourth power of wavefunction

$$IPR = \frac{1}{\sum_i {\psi_i}^4} \tag{1.3}$$

So, for bulk states IPR scale as L^2.

Similarly, the edge states whose probability density at the edges are highest and zero in

the bulk have the normalization condition:

$$\sum_{sites} |\Psi_{sites}|^2 \times Perimeter = 1 \tag{1.4}$$

or the wavefunction amplitude at the sites scale as $\frac{1}{\sqrt{4L}}$.The IPR in this case scale as L. A completely localized wavefunction has constant IPR value of 1.

So, smaller the value of IPR, the more localized the state is. In our calculations, we use this result to clearly identify the edge and bulk states. The bulk states do not conduct current only the edge state does. So, by counting the number of edge states we can figure out the conductivity of the system.

We will also use Density of states calculation in the thesis.The density of states peak at the energies of the landau levels and go to zero at the gaps. In the case of single impurity short range scattering , we see some new bound states being formed in the gaps between landau levels.Landau levels broaden. The density of states which is given by the imaginary part of the lattice green's function now becomes non zero in the gaps between landau levels. The Local density of states show increased density near the impurity and it tapers away from the impurity in a triangular fashion.

Chapter 2

Monolayer Graphene

Graphene is an allotrope of carbon having honeycomb lattice structure.It is a 2D material that has many properties that are of interest for not only basic science studies but also for technological purposes. It's effective tight binding nearest neighbour hopping low energy spectrum is the massless Dirac spectrum with linear dispersion relation instead of a parabolic dispersion[17]. The first brillouin zone is hexagonal with two inequivalent points called K and $K^{'}$ points on the edges of BZ. It is a gapless semi-metal(Conduction and valence bands touch at the dirac points) with density of states going to zero at the dirac point[17]. Graphene has four degrees of freedom - two spin degrees and two valley degrees of freedom(related to the two inequivalent atoms in the unit cell).

Energy levels are continuous in the absence of Magnetic field. In the presence of perpendicular magnetic field,the energy levels split into Landau levels with very large degeneracy.Interestingly the energy gaps between the Landau Levels scale as $\sqrt{n}$ where n is the Landau level index. The Integer Quantum Hall effect of graphene is anomalous with filling fractions of $\pm 2, \pm 6, \pm 10...$, which is in contrast to the filling fraction values of $\pm 1, \pm 2, ...$ and landau level gaps which scale as n in conventional 2D materials like GaAs [19] .

Monolayer graphene is a 2D sheet of carbon atoms arranged in hexagonal fashion.The hexagonal lattice is not a Bravis lattice. It can be thought of as two interpenetrating triangular lattices with atoms labelled A in one triangular lattice and B in the other. Nearest

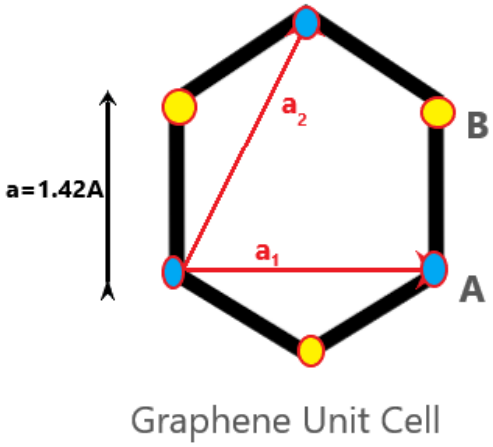

Figure 2.1: A unit cell of graphene with Lattice vectors marked. The choice of Lattice vectors is not unique. A and B type atoms are distinguished.

neighbours of an A type atom are B type and vice versa. We can take

$$\vec{a}_1 = \frac{a}{2}\left(3, \sqrt{3}\right); \vec{a}_2 = \frac{a}{2}\left(3, -\sqrt{3}\right) \tag{2.1}$$

as the lattice vectors.

$$\vec{b}_1 = \frac{2\pi}{3a}(1, \sqrt{3}); \vec{b}_2 = \frac{2\pi}{3a}(1, -\sqrt{3}) \tag{2.2}$$

These are the reciprocal lattice vectors. Brillouin zone of graphene is also hexagonal with two inequivalent and independent edge points which are also the dirac points in case of graphene.

$$\vec{K} = \left(\frac{2\pi}{3a}, \frac{2\pi}{3\sqrt{3}a}\right); \vec{K'} = \left(\frac{2\pi}{3a}, \frac{-2\pi}{3\sqrt{3}a}\right)$$

and $\vec{K'} = \vec{b_1} + \vec{b}_2 - \vec{K}$. The vectors that connect one B site to it's neighbouring A sites are:

$$\vec{\delta_1} = \frac{a}{2}\left(1, \sqrt{3}\right); \vec{\delta_2} = \frac{a}{2}\left(1, -\sqrt{3}\right); \vec{\delta_3} = a(-1, 0)$$

The Tight Binding Hamiltonian with nearest neighbour hopping can be written as

$$H(\vec{R}) = -t \sum_{<i,j>} \sum_{\sigma,} (a^{\dagger}_{\sigma,i}(\vec{R}) b_{\sigma,j}(\vec{R} + \vec{\delta}) + H.C) \tag{2.3}$$

where t is the hopping parameter(overlap integral) with an experimentally determined value of -2.7 e.V[11], $a_{\sigma,i}, b_{\sigma,i}$ are the annihilation operators that annihilates the electron located at the i^{th} site of type A and B both with spin σ respectively .$\vec{R}$ is the position of the i^{th} site and $\vec{\delta}$ is the vector from i^{th} site to it's nearest neighbours. H.C stands for hermitian conjugate. $\sum_{<i,j>}$ stands for summation over nearest neighbour sites. When there is no magnetic field, there is a discrete translation symmetry in the system which allows us to do a Fourier transform of the Hamiltonian into momentum space.

$$H(k) = \int_{k\ \epsilon 1^{st} BZ} \begin{pmatrix} a^{\dagger}(k) & b^{\dagger}(k) \end{pmatrix} \begin{pmatrix} 0 & -t\sum_i exp(i\vec{k}\cdot\vec{\delta_i}) \\ -t\sum_i exp(-i\vec{k}\cdot\vec{\delta_i}) & 0 \end{pmatrix} \begin{pmatrix} a(k) \\ b(k) \end{pmatrix} d^2k \tag{2.4}$$

where k is the wave number and $\vec{\delta_i}$'s are the 3 vectors that connect the nearest neighbours. We are interested in long wavelength limit or low energy limit $ka \ll 1$ where a is the lattice constant ($1.42\overset{\circ}{A}$). After doing some gauge transformations and taylor expanding the 2×2 matrix around the K and $K^{'}$ points separately, we get near $K^{'}$ point,

$$H_q = \hbar v_F \begin{pmatrix} 0 & -q_x + iq_y \\ -q_x - iq_y & 0 \end{pmatrix} \tag{2.5}$$

where $\vec{q} = \vec{k} - \vec{K'}$ and $|\vec{q}| \ll |\vec{K'}|$ and v_F is called as the fermi velocity. We can follow same procedure near K point to get

$$H_q = \hbar v_F \begin{pmatrix} 0 & q_x + iq_y \\ q_x - iq_y & 0 \end{pmatrix} \tag{2.6}$$

around K point. Using pauli matrices and combining the two results and writing succinctly,

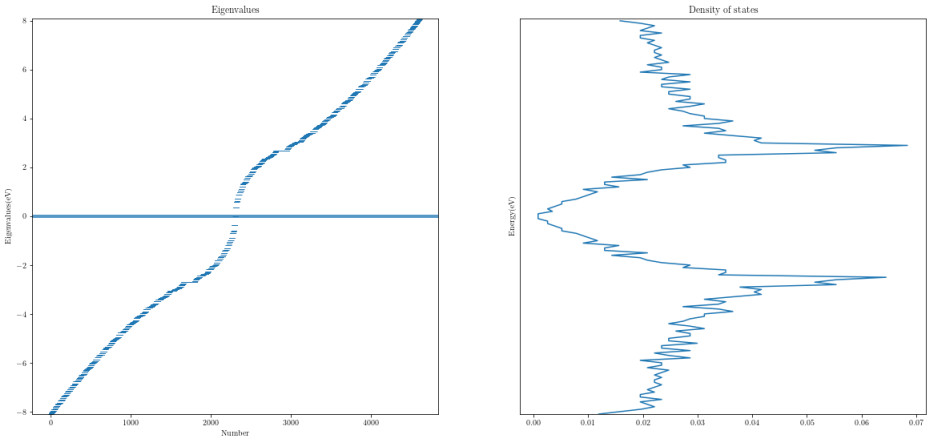

Figure 2.2: Eigenvalues for a Graphene lattice of small size (left) and corresponding density of states (right) simulated.

we get

$$H_q = \hbar v_F \begin{pmatrix} \vec{\sigma} \cdot \vec{q} & 0 \\ 0 & -\vec{\sigma}^{\star} \cdot \vec{q} \end{pmatrix} \tag{2.7}$$

This gives

$$E_{\pm}(\vec{q}) = \hbar v_F |\vec{q}| \tag{2.8}$$

If we compare this result to the massless particle's energy dispersion

$$E = \hbar c k \tag{2.9}$$

we can clearly see that both the results are similar but in case of graphene, the speed is v which is of the order of 10^6 unlike c which is of the order of 10^8. This fact enables us to observe many relativistic particle phenomena in a condensed matter system.

H_q is a 4×4 block matrix with first block being the effective Hamiltonian near K valley and the second block, the Hamiltonian near K' valley. $\vec{\sigma}$ is the pauli vector. The matrix is written in the wavefunction basis: $\begin{pmatrix} \Psi_A^K & \Psi_B^K & \Psi_A^{K'} & \Psi_B^{K'} \end{pmatrix}^T$

Figure 2.2 shows the energy spectrum for Graphene in the absence of magnetic field. The

energies around zero increase or decrease linearly corresponding to the Dirac spectrum. The higher energies do not scale linearly indicating that Dirac spectrum is only applicable for low energy states. The figure on the right is the Density of states calculation. It has a v shape and goes to zero at $E = 0$ making graphene a semi metal which has no gap between valence band and conduction band but also no states present at the Fermi energy.

In the presence of a perpendicular magnetic field, we can implement the effect of magnetic field into the Hamiltonian by doing the peirels substitution that takes momentum operator into it's gauge invariant form which effectively is:

$$\hbar q_i \longrightarrow \hbar q_{gi} = \hbar q_i + eA_i \qquad i = (x, y) \tag{2.10}$$

where $\boldsymbol{A}(x, y)$ is the Gauge potential with $\nabla \times \boldsymbol{A} = \boldsymbol{B}$. We can fix the gauge by choosing Landau Gauge: $\boldsymbol{A} = (By, 0)$. Since $\boldsymbol{A} = \begin{pmatrix} -By & 0 \end{pmatrix}$, the Hamiltonian commutes with p_x i.e, $[H, p_x] = 0$. So p_x is a good quantum number. i.e, the single particle eigenstates can be chosen to be eigenstates of p_x also. Solutions near K valley for $H\Psi^K = E\Psi^K$

$$\hbar \begin{bmatrix} 0 & q_{gx} - \imath q_{gy} \\ q_{gx} + \imath q_{gy} & 0 \end{bmatrix} \begin{bmatrix} \Psi_A^K \\ \Psi_B^K \end{bmatrix} = E \begin{bmatrix} \Psi_A^K \\ \Psi_B^K \end{bmatrix} \tag{2.11}$$

$$\implies \hbar \left(q_{gx} - \imath q_{gy}\right) \Psi_B^K = E\Psi_A^K \text{ and } \hbar \left(q_{gx} + \imath q_{gy}\right) \Psi_A^K = E\Psi_B^K \tag{2.12}$$

Combining them we get

$$\hbar^2 \left(q_{gx} - \imath q_{gy}\right) \left(q_{gx} + \imath q_{gy}\right) \Psi_A^K = E^2 \Psi_A^K \tag{2.13}$$

$$\hbar^2 \left(q_{gx} + \imath q_{gy}\right) \left(q_{gx} - \imath q_{gy}\right) \Psi_B^K = E^2 \Psi_B^K \tag{2.14}$$

Simplifying the above equations,

$$\hbar^2 v_F^2 \left(q_{gx}^2 + q_{gy}^2 + \imath \left[q_{gx}, q_{gy}\right]\right) \Psi_A^K = E^2 \Psi_A^K$$

$$\hbar^2 v_F^2 \left(q_{gx}^2 + q_{gy}^2 - \imath \left[q_{gx}, q_{gy}\right]\right) \Psi_B^K = E^2 \Psi_B^K$$

$$\left[q_{gx}, q_{gy}\right] = \left[\left(q_x - \frac{eB}{\hbar} y\right), q_y\right] = -\frac{eB}{\hbar}\left[y, q_y\right] = -\frac{eB}{\hbar^2}\left[y, p_y\right] = -\imath \frac{eB}{\hbar}$$

$$\hbar^2 v_F^2 \left(q_x^2 + q_y^2\right) \Psi_A^K = \left(E^2 - eB\hbar v_F^2\right) \Psi_A^K$$

$$\hbar^2 v_F^2 \left(q_x^2 + q_y^2\right) \Psi_B^K = \left(E^2 + eB\hbar v_F^2\right) \Psi_B^K$$

$$\Psi_{A,B}^K (x, y) \equiv \Phi_{A,B}^K \left(y - \frac{\hbar k_x}{eB}\right) e^{\imath k_x x}$$

Define

$$\overline{y} = y - \frac{\hbar k_x}{eB}$$

Then,

$$\left(q_x - \frac{eB}{\hbar} y\right) \Psi_{A,B}^K (x, y) = \left(-\imath \partial_x - \frac{eB}{\hbar} y\right) \Phi_{A,B}^K \left(y - \frac{\hbar k_x}{eB}\right) e^{\imath k_x x}$$

$$= \left(k_x - \frac{eB}{\hbar} y\right) \Phi_{A,B}^K \left(y - \frac{\hbar k_x}{eB}\right) e^{\imath k_x x}$$

$$= \frac{eB}{\hbar} \left(\frac{\hbar}{eB} k_x - y\right) \Psi_{A,B}^K (x, y) = -\frac{eB}{\hbar} \overline{y} \Psi_{A,B}^K (x, y)$$

$$\implies q_x^2 \Psi_{A,B}^K (x, y) = \frac{e^2 B^2}{\hbar^2} \overline{y}^2 \Psi_{A,B}^K (x, y)$$

$$\left(e^2 B^2 \overline{y}^2 - \hbar^2 \partial_{\overline{y}}^2\right) \Phi_A^K = \left(\frac{E^2}{v_F^2} - eB\hbar\right) \Phi_A^K$$

$$\left(e^2 B^2 \overline{y}^2 - \hbar^2 \partial_y^2\right) \Phi_B^K = \left(\frac{E^2}{v_F^2} + eB\hbar\right) \Phi_B^K$$

This is like Quantum Harmonic oscillator with

$$m = \tfrac{1}{2} \text{ and } \omega = 2eB$$

$\hbar\left(q_{gx} + \imath q_{gy}\right)$ is the raising operator. i.e, it raises the value of E^2.

Eigenvalues are

$$\hbar\omega\left(n + \tfrac{1}{2}\right) = \text{ where } n = 0, 1, 2\ldots$$

$$\implies \tfrac{E^2}{v_F^2} - eB\hbar = 2\hbar eB\left(n_A + \tfrac{1}{2}\right) \text{ and } \tfrac{E^2}{v_F^2} + eB\hbar = 2\hbar eB\left(n_B + \tfrac{1}{2}\right)$$

$$E = \pm v_F\sqrt{2\hbar eB\left(n_A + 1\right)} = \pm v_F\sqrt{2\hbar eBn_B}$$

$$\implies n_B = n_A + 1 = n$$

$$\Phi_A^K\left(\overline{y}\right) = \chi_{n-1}\left(\overline{y}\right)$$

$$\Phi_B^K\left(\overline{y}\right) = e^{\imath c}\chi_n\left(\overline{y}\right)$$

Since $\hbar\left(q_{gx} + \imath q_{gy}\right)$ is the raising operator,

$$\hbar\left(q_{gx} + \imath q_{gy}\right)\chi_n = \sqrt{n+1}\chi_{n+1}\left(\overline{y}\right)$$

There might be additional multiplicative constants in the LHS. To find this out, assume χ_n and χ_{n+1} are normalized, and then try to find the norm of $\hbar\left(q_x + \imath q_y\right)\chi_n$

$$\hbar\begin{bmatrix} 0 & q_{gx} - \imath q_{gy} \\ q_{gx} + \imath q_{gy} & 0 \end{bmatrix}\begin{bmatrix} \chi_{n-1}\left(\overline{y}\right)e^{\imath kx} \\ e^{\imath c}\chi_n\left(\overline{y}\right)e^{\imath kx} \end{bmatrix} = \pm v_F\sqrt{2\hbar eBn}\begin{bmatrix} \chi_{n-1}\left(\overline{y}\right)e^{\imath kx} \\ e^{\imath c}\chi_n\left(\overline{y}\right)e^{\imath kx} \end{bmatrix} \tag{2.15}$$

$$\implies \begin{bmatrix} \sqrt{n}e^{\imath c}\chi_{n-1}\left(\overline{y}\right)e^{\imath kx} \\ \sqrt{n}\chi_n\left(\overline{y}\right)e^{\imath kx} \end{bmatrix}$$

From now on we skip the subscript g in wavevector components and understand q_x means q_{gx}. Defining

$$\pi = p_x + ip_y = \hbar\,(q_x + \imath q_y)$$

Solving for Φ_B^K, we get

$$\frac{1}{2m}(\frac{E^2}{{v_2}_F} + \hbar eB)\Phi_B^K = (\frac{\tilde{K}}{2}(y - y_0)^2 + \frac{p_y^2}{2m})\Phi_B^K$$

where $\tilde{K} = \frac{eB}{\sqrt{m}}; y_0 = \frac{-p_x}{eB}$; Solution for RHS is : $\hbar\omega_c(n + \frac{1}{2})$ where $\omega_c = eB/m$.This finally gives us

$$E_n = \pm v_F\sqrt{2\hbar eBn} \tag{2.16}$$

where $n = 0, \pm1, \pm2, ...$ is the nth Landau level index. Similarly solving for Φ_A^K, we would get,

$$E = sgn(n')v_F\sqrt{2(|n'| + 1)\hbar eB} \tag{2.17}$$

As both Φ_A^K,and Φ_B^K should give same energy eigenvalue, we must have $n' = n - 1$ With this,

$$\Psi_{n,q}^K = Ae^{-iqx}\begin{pmatrix} sgn(n)||n| - 1> \\ ||n|> \\ 0 \\ 0 \end{pmatrix} \tag{2.18}$$

where, A is normalization constant and $||n|>$ is the number operator eigenstate. It can

be expressed in terms of Hermite polynomials as:

$$\Psi^{K}_{n,q} = Ae^{-iqx} \begin{pmatrix} sgn(n)\phi_{|n|-1,q} \\ \phi_{|n|,q} \\ 0 \\ 0 \end{pmatrix} \tag{2.19}$$

Near the K' point, same procedure can be followed. It can be easily written down by just changing the result near K point by changing A and B indices. i,e.

$$\Psi^{K'}_{n,q} = Ae^{-iqx} \begin{pmatrix} 0 \\ 0 \\ \phi_{|n|,q} \\ sgn(n)\phi_{|n|-1,q} \end{pmatrix} \tag{2.20}$$

This is the result for continuum model of Graphene. Landau level energies increasing as $\sqrt{n}$ is in contrast to the conventional 2D materials where landau level energies increase as n. The $n = 0$ Landau level is special in the sense that the wavefunction is completely localized on only one type of sublattice.

We studied the infinite lattice system or periodic boundary conditions till now. In a realistic scenario,the system will have edges.Graphene can mainly have two types of edges.We find that for the case of the zigzag edge termination, both monolayer and bilayer ribbons, because of chirality, in single and few mode regime, remain insensitive to defects situated close to the edges. On the other hand, the transport properties of both armchair monolayer and bilayer nanoribbons is heavily affected by even a small edge defect concentration. This behaviour of vastly different properties is related to the effective boundary conditions at the edges, which couple K and K' valleys for zigzag nanoribbons and does not couple the two valleys in case of armchair nanoribbons. When the defect concentration is very large or there are multiple modes, in that regime, the difference in transport properties of two edges diminishes[18]. In a hexagonal lattice like that of Graphene, short range scatterers are believed to be present almost always. They can scatter states near one valley to the other.

In this chapter we studied continuum model. We also study discrete Harper Hofstadter lattice model for Graphene for reasons that are explained in the chapter 4.

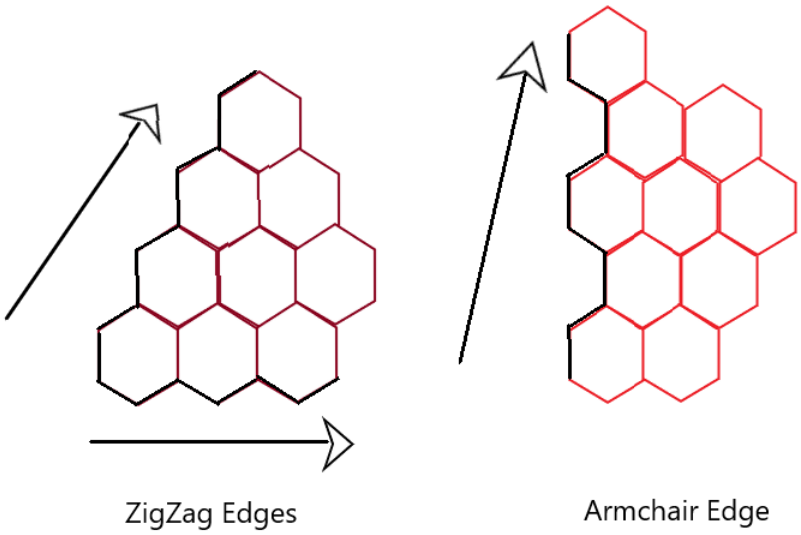

Figure 2.3: Zig-zag and armchair edges in Graphene

Chapter 3

Bilayer Graphene

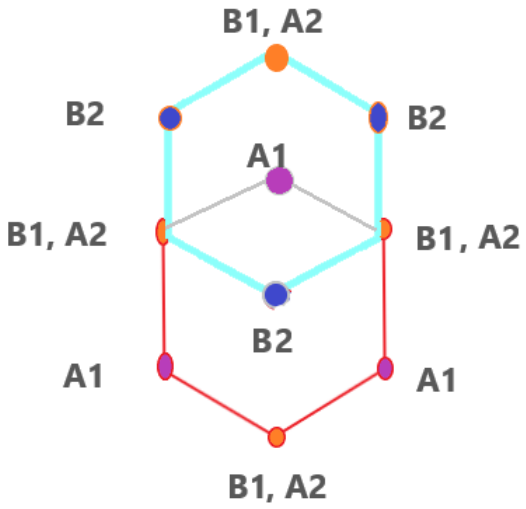

Figure 3.1: Bilayer Graphene in Bernal Stacking. A1, B1 corresponds to the atoms in lower layer and A2 and B2 corresponds to the atoms in upper layer. A2 atoms are exactly on top of B1 atoms.

Bilayer Graphene in Bernal stacking is shown in figure 3.1. It is the most common type of arrangement in BLG. There are two layers. The interlayer distance is $3.4\mathring{A}$. The label 1 corresponds to lower layer and 2 corresponds to upper layer.

In the tight binding description, a tight binding Hamiltonian can be written for Bilayer

Graphene that includes hopping within the layer and also the interlayer coupling between B1 and A2 sites in Bernal stacking.

$$H = -\gamma_0(\sum_{<i,j>_1} a_{1j}^\dagger b_{1i} + \sum_{<i,j>_1} a_{2j}^\dagger b_{2i}) + \gamma_1 \sum_{j_c} a_{2j_c}^\dagger b_{1j_c} - \gamma_3 \sum_{<i,j>} a_{1j}^\dagger b_{2i} + \gamma_4(\sum_{<i,j>} a_{1j}^\dagger b_{2i} + \sum_{<i,j>} b_{1j}^\dagger a_{2i}) + H.C \tag{3.1}$$

The tight binding parameters are:

$$\gamma_0 = - < \phi_{A1}|H|\phi_{B1} >; \gamma_1 =< \phi_{A2}|H|\phi_{B1} >; \gamma_3 = - < \phi_{A1}|H|\phi_{B2} >; \gamma_4 =< \phi_{A1}|H|\phi_{A2} >$$

Where ϕ's are atomic wavefunctions. Defining the fourier transforms of operators as:

$$a_1(\vec{k}) = \sum_j e^{i\vec{k}\cdot\vec{R}_j} a_{1j}; b_1(\vec{k}) = \sum_j e^{i\vec{k}\cdot\vec{R}_j} b_{1j}$$

$$a_2(\vec{k}) = \sum_j exp(i\vec{k}\cdot\vec{R}_j) a_{2j}; b_2(\vec{k}) = \sum_j e^{i\vec{k}\cdot\vec{R}_j} b_{2j}$$

$$H(k) = \int_{k\epsilon BZ} (a_1^\dagger, b_1^\dagger, a_2^\dagger, b_2^\dagger) h(k) \begin{pmatrix} a_1 \\ b_1 \\ a_2 \\ b_2 \end{pmatrix} \tag{3.2}$$

Fixing the centre to be at A1,

$$R^{A1} = R; R^{b1} = R + \delta_{AB}; R^{A2} = R + \delta_{AB}; R^{B2} = R - \delta_{AB}$$

$$h(k) = \begin{pmatrix} \epsilon_{A1} & -\gamma_0 f(k) & \gamma_4 f(k) & -\gamma_3 f(k)^\dagger \\ -\gamma_0 f(k)^\dagger & \epsilon_{B1} & \gamma_1 & \gamma_4 f(k) \\ \gamma_4 f(k)^\dagger & \gamma_1 & \epsilon_{A2} & -\gamma_0 f(k) \\ -\gamma_3 f(k) & \gamma_4 f(k)^\dagger & -\gamma_0 f(k)^\dagger & \epsilon_{B2} \end{pmatrix} \tag{3.3}$$

where we have included parameters of on- site energies $\epsilon_{A,j}, \epsilon_{B,j}$ such that,

$$\epsilon_{A1} = \frac{1}{2}(-U + \delta_{AB})$$

$$\epsilon_{B1} = \frac{1}{2}(-U - \delta_{AB} + 2\Delta^{'})$$

$$\epsilon_{A2} = \frac{1}{2}(U + \delta_{AB} + 2\Delta^{'})$$

$$\epsilon_{B2} = \frac{1}{2}(U - \delta_{AB})$$

$$U = \frac{1}{2}[(\epsilon_{A1} + \epsilon_{B1}) - (\epsilon_{A2} + \epsilon_{B2})]$$

U is the inter layer difference in energy which is like a chemical potential difference.

$$\Delta' = \frac{1}{2}[(\epsilon_{B1} + \epsilon_{A2}) - (\epsilon_{A1} + \epsilon_{B2})]$$

Δ' is the difference of energy between dimer and non dimer atoms.

$$\delta_{AB} = \frac{1}{2}[(\epsilon_{A1} + \epsilon_{A2}) - (\epsilon_{B1} + \epsilon_{B2})]$$

This is the difference between A type and B type atoms.

By putting parameters values as $\gamma_0 = 3.16eV, \gamma_1 = 0.381eV, \gamma_3 = 0.138eV, \epsilon_{A1} = \epsilon_{B2} = U = \delta_{AB} = 0; \epsilon_{B1} = \epsilon_{A2} = \Delta' = 0.022eV$.

We can plot the band structure with these parameters.

In the band structure, we see that two kinds of bands are formed. Near the K points, we can find two bands touching zero. They are formed from hopping between A1 and B2. The other two are called bonding and anti bonding bands as they are formed because of hybridization of the dimer bond. They don't touch zero on the X-axis.

Consider

$$\vec{p} = \hbar\vec{k} - \hbar\vec{k_\xi}$$

As was seen in Monolayer case, in the continuum limit, $f(k)$ near $\vec{k_\xi}$ point is $-\frac{3a}{2\hbar}(\xi p_x - ip_y)$. Defining $\vec{\pi} = \xi p_x + ip_y$; $\pi^\dagger = \xi p_x - ip_y$ and $v = \frac{3a\gamma_0}{2\hbar}$, Then,

$$h(k) = \begin{pmatrix} \epsilon_{A1} & v\pi^\dagger & -v\pi^\dagger & v_3\pi \\ v\pi & \epsilon_{B1} & \gamma_1 & -v_4\pi^\dagger \\ -v_4\pi & \gamma_1 & \epsilon_{A2} & v\pi^\dagger \\ v_3\pi^\dagger & -v_4\pi & v\pi & \epsilon_{B2} \end{pmatrix} \tag{3.4}$$

As it stands, this is quite general and complicated. To get a simple analytic solution, we make some assumptions.Neglect terms with γ_4 and put $\epsilon_{A1} = \epsilon_{B1} = -\frac{U}{2}; \epsilon_{A2} = \epsilon_{B2} = \frac{U}{2}$; So,

$$h(k) = \begin{pmatrix} -\frac{U}{2} & v\pi^\dagger & 0 & v_3\pi \\ v\pi & -\frac{U}{2} & \gamma_1 & 0 \\ 0 & \gamma_1 & \frac{U}{2} & v\pi^\dagger \\ v_3\pi^\dagger & 0 & v\pi & \frac{U}{2} \end{pmatrix} \tag{3.5}$$

Now we find the eigenvalues of this matrix. In the characteristic equation, The E^3,E terms become zero.So, we can solve for E_α^2,

$$E_\alpha^2 = \frac{\gamma_1^2}{2} + \frac{U^2}{4} + (v^2 + \frac{v_3^2}{2})p^2 + (-1)^\alpha\sqrt{\Gamma} \tag{3.6}$$

where,

$$\Gamma = \frac{1}{4}(\gamma_1^2 - v_3^2p^2)^2 + v^2p^2[\gamma_1^2 + U^2 + v_3^2p^2] + 2\xi\gamma_1v_3v^2p^3cos3\varphi \tag{3.7}$$

$$\varphi = tan^{-1}(\frac{p_y}{p_x})$$

If we want only low energy bands($\alpha = 1$), we use a simple general procedure to obtain effective low energy Hamiltonian: Consider,

$$h = \begin{pmatrix} h_\theta & u \\ u^\dagger & h_\chi \end{pmatrix} \tag{3.8}$$

where h_θ is the block that contain low energies and h_χ is the high energy block.

$$\theta = \begin{pmatrix} \psi_{A1} \\ \psi_{B2} \end{pmatrix}$$

$$\chi = \begin{pmatrix} \psi_{A2} \\ \psi_{B1} \end{pmatrix}$$

$$\begin{pmatrix} h_\theta & u \\ u^\dagger & h_\chi \end{pmatrix} \begin{pmatrix} \theta \\ \chi \end{pmatrix} = E \begin{pmatrix} \theta \\ \chi \end{pmatrix}$$

$$\implies u^\dagger \theta + h_\chi \chi = E\chi$$

Solving for χ,

$$\chi = (E - h_\chi)^{-1} u^\dagger \theta$$

Putting this in the first equation,

$$[h_\theta + u(E - h_\chi)^{-1} u^\dagger]\theta = E\theta \tag{3.9}$$

As we want those E which are of low energies, Eigenvalues of $h_\chi \gg E$. So, expanding in the parameter $\frac{E}{h_\chi}$

$$(E - h_\chi)^{-1} = h_\chi^{-1}(\frac{E}{h_\chi} - 1)^{-1} = h_\chi^{-1}(-1 - h_\chi^{-1}E) = -h_\chi^{-1} - h_\chi^{-2}E \tag{3.10}$$

So, rearranging this,

$$[h_\theta + u h_\chi^{-1} u^\dagger]\theta \approx E(1 + u h_\chi^{-2} u^\dagger)\theta \tag{3.11}$$

Call $(1 + u h_\chi^{-2} u^\dagger)$ as S.

Now we do a transformation, $\Phi = S^{\frac{1}{2}}\theta$

$$\implies [h_\theta + uh_\chi^{-1}u^\dagger]S^{-\frac{1}{2}}\Phi = ES^{\frac{1}{2}}\Phi$$

or

$$S^{-\frac{1}{2}}[h_\theta + uh_\chi^{-1}u^\dagger]S^{-\frac{1}{2}}\Phi = E\Phi \tag{3.12}$$

This transformation was done to have a normalization

$$\Phi^\dagger\Phi = \theta^\dagger S\theta = \theta^\dagger(1 + uh_\chi^{-2}u^\dagger)\theta \approx \theta^\dagger\theta + \chi^\dagger\chi$$

So,

$$h_{eff} \approx S^{-\frac{1}{2}}[h_\theta - uh_\chi^{-1}u^\dagger]S^{-\frac{1}{2}} \tag{3.13}$$

For the case of Bilayer graphene, we first write h in the basis : $(A1, B2, A2, B1)$ Then,

$$h = \begin{pmatrix} \epsilon_{A1} & v_3\pi & -v_4\pi^\dagger & v\pi^\dagger \\ v_3\pi^\dagger & \epsilon_{B2} & v\pi & -v_4\pi^\dagger \\ -v_4\pi & v\pi^\dagger & \epsilon_{A2} & \gamma_1 \\ v\pi & -v_4\pi^\dagger & \gamma_1 & \epsilon_{B1} \end{pmatrix} \tag{3.14}$$

$$h_\theta = \begin{pmatrix} \epsilon_{A1} & v_3\pi \\ v_3\pi^\dagger & \epsilon_{B2} \end{pmatrix} \tag{3.15}$$

$$h\chi = \begin{pmatrix} \epsilon_{A2} & \gamma_1 \\ \gamma_1 & \epsilon_{B1} \end{pmatrix} \tag{3.16}$$

$$u = \begin{pmatrix} -v_4\pi^\dagger & v\pi^\dagger \\ v\pi & -v_4\pi^\dagger \end{pmatrix}$$

$$u^\dagger = \begin{pmatrix} -v_4\pi & v\pi^\dagger \\ v\pi & -v_4\pi^\dagger \end{pmatrix}$$

To calculate the $S^{-\frac{1}{2}}$ etc. it would be a lengthy calculation. So we make some reasonable approximations here such as:

$$\gamma_0, \gamma_1 \gg |E|, vp, |\gamma_3|, |\gamma_4|, |U|, |\Delta'|, |\delta_{AB}|$$

Then keeping only terms that are linear in small parameters and quadratic in momentum, we get

$$\hat{h}_2 = \hat{h}_0 + \hat{h}_w + \hat{h}_4 + \hat{h}_\Delta + \hat{h}_U + \hat{h}_{AB} \tag{3.17}$$

where,

$$\hat{h}_0 = -\frac{1}{2m}\begin{pmatrix} 0 & (\pi^\dagger)^2 \\ \pi^2 & 0 \end{pmatrix} \tag{3.18}$$

which is the massless chiral term.

$$\hat{h}_w = v_3\begin{pmatrix} 0 & \pi \\ \pi^\dagger & 0 \end{pmatrix} - \frac{v_3 a}{4\sqrt{3}\hbar}\begin{pmatrix} 0 & (\pi^\dagger)^2 \\ \pi^2 & 0 \end{pmatrix} \tag{3.19}$$

which is the trigonal warping term.

$$\hat{h}_4 = \tfrac{2vv_4}{\gamma_1}\begin{pmatrix} \pi^\dagger\pi & 0 \\ 0 & \pi\pi^\dagger \end{pmatrix}$$

$$\hat{h}_\Delta = \tfrac{\Delta' v^2}{\gamma_1^2}\begin{pmatrix} \pi^\dagger\pi & 0 \\ 0 & \pi\pi^\dagger \end{pmatrix}$$

This is the electron hole asymmetry inducing term.

$$\hat{h}_U = \tfrac{-U}{2}\begin{pmatrix} 1 & 0 \\ 0 & -1 \end{pmatrix} + \tfrac{Uv^2}{\gamma_1^2}\begin{pmatrix} \pi^\dagger\pi & 0 \\ 0 & -\pi\pi^\dagger \end{pmatrix}$$

$$\hat{h}_{AB} = \frac{\delta_{AB}}{2}\begin{pmatrix} 1 & 0 \\ 0 & -1 \end{pmatrix}$$

This term produces band gap and $m = \frac{\gamma_1^2}{2v^2}$. Studying these perturbations to the Hamiltonian, is very insightful. For example, the trigonal warping term mixes a landau level with the landau level index 3 more than it's index.

Consider the low energy Hamiltonian h_0. We know that $\vec{\pi} = \xi p_x + i p_y$; $\pi^\dagger = \xi p_x - i p_y$. Solving the Eigenvalue Equation $h_0\Psi = E\Psi$,

$$-\frac{1}{2m}\begin{pmatrix} 0 & (\pi^\dagger)^2 \\ (\pi)^2 & 0 \end{pmatrix}\begin{pmatrix} \psi^{A1} \\ \psi^{B2} \end{pmatrix} = E\begin{pmatrix} \psi^{A1} \\ \psi^{B2} \end{pmatrix} \tag{3.20}$$

We will get,

$$-\frac{1}{2m}(\pi^\dagger)^2\psi^{B2} = E\psi^{A1} \tag{3.21}$$

$$-\frac{1}{2m}(\pi)^2\psi^{A1} = E\psi^{B2} \tag{3.22}$$

Decoupling these equations,

$$\frac{1}{4m^2}(\pi^\dagger)^2(\pi)^2\psi^{A1} = E^2\psi^{A1}\frac{1}{4m^2}(\pi)^2(\pi^\dagger)^2\psi^{B2} = E^2\psi^{B2} \tag{3.23}$$

Noticing that momentum operators commute when the magnetic field is absent, we can freely move the operators to get

$$E^2 = \frac{(|p|^2)^2}{4m^2}$$

or

$$E = \pm\frac{|p|^2}{2m} \tag{3.24}$$

These solutions are well known parabolic dispersion relation unlike the linear dispersion in case of Monolayer Graphene.

The Eigenfunctions are given by:

$$\Psi = \frac{1}{\sqrt{2}} e^{i\boldsymbol{k}\cdot\boldsymbol{r}} \begin{pmatrix} 1 \\ \mp e^{-2\iota\xi\phi} \end{pmatrix}$$

In presence of magnetic field, we will have peirels substution. Then the momentum poerators no longer commute. We will consider the case of Landau Gauge $\boldsymbol{A} = (0, -Bx, 0)$.

$$[p_{gx}, p_{gy}] = [p_x, p_y - eBx] = -eB[p_x, x] - i\hbar eB$$

$$\boldsymbol{\pi} = -\iota\hbar\nabla = -\iota\xi\hbar\partial_x + \hbar\partial_y - \iota eBx$$

$$\boldsymbol{\pi}^\dagger = -\iota\xi\hbar\partial_x - \hbar\partial_y + \iota eBx$$

When we introduce this modification in eq.3.23, and using the definition of commutator operator, $\pi^\dagger\pi = [\pi^\dagger, \pi] + \pi\pi^\dagger$, and then following the same line of arguments as was done for monolayer, we arrive at the relation:

$$H^2\Psi = \frac{4\hbar^2 v_F^2}{l_B^2} \begin{pmatrix} (n+1)(n+2) \\ n^{'}(n-1)^{'} \end{pmatrix} \Psi \tag{3.25}$$

Requiring that the energies corresponding to both components of wavefunction be the same, we arrive at the result for landau levels for bilayer graphene:

$$E_{n,\pm} = \pm\hbar\frac{eB}{m}\sqrt{|n|(|n|-1)} \qquad , n \geq 2. \tag{3.26}$$

As we have no y dependence in Gauge field, we can apply Bloch theorem to obtain plane wave solutions in y direction and a combination of Harmonic Oscillator functions in x direction in the same method we used in finding the landau levels of monolayer graphene.

We obtain

$$\Psi_n(x, y) = H_n(\frac{x}{l_B} - k_y l_B) e^{[-\frac{1}{2}(\frac{x}{l_B} - k_y l_B)^2 + ik_y y]} \tag{3.27}$$

up to a normalization constant. The H_n are the hermite polynomials that are the solutions

of Harmonic oscillator problem. It is trivial to see that for $\xi = +1$ (K point), the $\boldsymbol{\pi}$ acts as the lowering operator on $\Psi_n(x, y)$ and $\boldsymbol{\pi}^\dagger$ acts as the raising operator with the condition that $\boldsymbol{\pi}\Psi_0(x, y) = 0$. For $K^{'}$ valley, the roles are reversed.

$E_{n,\pm} = 0$ for $n = 0, 1$. So we get an eightfold degeneracy in landau level at $E = 0$.

Chapter 4

Hofstadter Model

In condensed matter physics, when we are interested in finding the spectrum of a system, we first consider a unit cell and solve the Hamiltonian for that unit cell. The smaller the unit cell is, the smaller the Hamiltonian that needs to be diagonalized which in turn means faster computation. When a magnetic field is introduced, it reduces the symmetry of the system. The unit cell size will increase depending on the exact nature of the magnetic field introduced. The practical problem we face in doing numerical calculations is that of extremely large number of lattice sites that we need to take in order to get a periodic system if the magnetic field is smaller. We will find in this chapter why smaller Magnetic fields require larger number of lattice sites. On the other hand, it is very hard to produce large magnetic fields in laboratory. This means, experimentally, we are more likely to encounter the low magnetic field regime. We, in this project focus on numerical study which becomes exponentially more time consuming if we choose to study the experimentally accessible low energy continuum limit. In the regime of large magnetic fields, our numerical calculations become less demanding. This regime for lattice models is called Harper-Hofstadter regime.

The condition for continuum model regime is $ka << 1$ which was the subject of chapter 2. When this relation no longer holds, we enter Harper-Hofstadter regime. Now, we shall describe Hofstadter regime briefly.

The presence of magnetic field adds a phase to the wave function which depends on vector potential. Within the tight binding model, we can transfter that phase from wavefunction

onto the hopping parameter[5] to get:

$$t_{ij} = t \longrightarrow te^{-i\frac{e}{\hbar}2\pi \int_i^j \vec{A}(x,y)\cdot\vec{dl}} \tag{4.1}$$

where Hopping parameter in the presence of magnetic field for the hopping from i^{th} site to j^{th} site is given by the above equation and A is the gauge field usually in Landau or symmetric gauge.

This substitution can be rigorously proved and is similar to the Aharonov Bohm phase acquired when a charged particle undergoes a circular motion in presence of magnetic field.

In case of square lattice, the nearest neighbour hopping hamiltonian can be written as composed of translation operators. In the absence of magnetic field, those operators commute among themselves and with the Hamiltonian. The Bloch wave ansatz can then be used for wavefunctions. But when $B \neq 0$, magnetic field enters the Hamiltonian in the form of Peirels phases as discussed earlier. It breaks the translation symmetry. The translation operators do not commute among themselves nor with the Hamiltonian. We can define magnetic translation operators which are determined by the flux passing through each plaquette and the peirels phases such that they commute with Hamiltonian.

In general, the magnetic translation operators do not commute with each other. When the magnetic flux is homogenous i.e, the flux passing through each plaquette is the same, then there exists a case when we can restore the translation symmetry in the system. When we compute $[T_x, T_y{}^q]$, they generally do not commute but if we impose the condition that they commute, we get the condition for commutation to be that magnetic flux (in the units of flux quantum) is a rational number $\frac{p}{q}$. When this condition is met, we can take q unit cells in y direction which is called magnetic unit cell as the new translationally invariant unit cell and apply Bloch theorem. When we plot the graph of energy vs flux, the resulting figure is called as Hofstadter Butterfly which is a fractal.

In case of Graphene, we consider the figure 4.1. The situation is more involved as Graphene atoms have three nearest neighbours and there is a sublattice degree of freedom as well.

We have the freedom to choose a gauge that is most convenient for us. We define magnetic

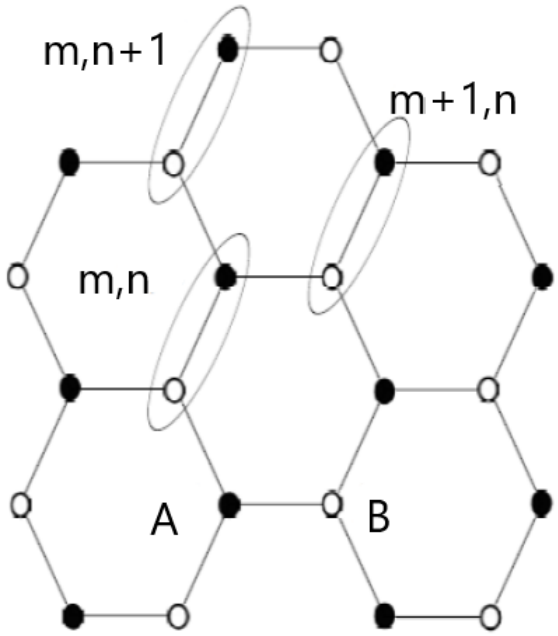

Figure 4.1: Labelling scheme of unit cells and atoms.

hopping operators T_j,$(j = 1, 2, 3)$ such that:

$$T_1\psi_{m,n} = \begin{pmatrix} \psi^B_{m,n} \\ \psi^A_{m,n} \end{pmatrix}$$

$$T_2\psi_{m,n} = \begin{pmatrix} \psi^B_{m+1,n} \\ \psi^A_{m-1,n} \end{pmatrix}$$

$$T_3\psi_{m,n} = \begin{pmatrix} e^{-2\pi\iota\Phi m}\psi^B_{m,n+1} \\ e^{2\pi\iota\Phi m}\psi^A_{m,n-1} \end{pmatrix}$$

This fixes our gauge and the definition of magnetic hopping operators. Recalling the nearest neighbour tight binding Hamiltonian, we write equation 2.3 as:

$$H = \sum_j T_j \tag{4.2}$$

We have chosen the gauge in which H is translationally invariant in the n direction and in m direction it is periodic with q unit cells if flux is $\frac{p}{q}$ similar to the square lattice case. Define the fourier transform of a bloch wavefunction in the translationally invariant direction

as:

$$\Psi_{m,n} = \int_0^{2\pi} dk \Psi_m(k) e^{\iota kn}$$

With this definition and the fourier transform of H in n direction, we get Harper equation for honeycomb lattice as:

$$(H(k)\Psi(k))_m = \begin{pmatrix} 0 & 0 \\ 1 & 0 \end{pmatrix} \begin{pmatrix} \psi^A_{m-1} \\ \psi^B_{m-1} \end{pmatrix} + \begin{pmatrix} 0 & 1 + e^{\iota(k-2\pi\Phi m)} \\ 1 + e^{-\iota(k-2\pi\Phi m)} & 0 \end{pmatrix} + \begin{pmatrix} 0 & 1 \\ 0 & 0 \end{pmatrix} \begin{pmatrix} \psi^A_{m+1} \\ \psi^B_{m+1} \end{pmatrix} \tag{4.3}$$

We can solve this equation for different values of m and plotting the energies versus flux, we will obtain Hofstadter Butterfly for honeycomb lattice.

The connection between hall conductance and Hofstadter spectrum is that the conductance in the r^{th} spectral gap is given by a Diophantine equation:

$$r = \sigma_H \cdot p + s \cdot q \tag{4.4}$$

4.1 Peirels Phases for square and Honeycomb Lattices

Consider a square lattice as shown in the figure 4.2.

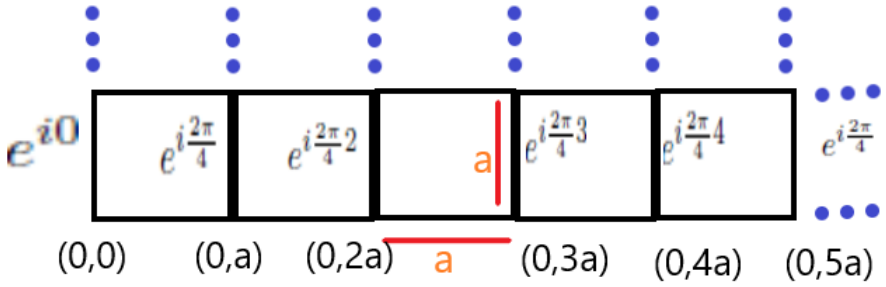

Figure 4.2: Describing peirels phase for square lattice.

Assuming $\mathbf{\Phi} = \frac{\mathbf{\Phi_0}}{4}$ flux passes through one plaquette in the square lattice and fixing the guage to be Landau gauge $\boldsymbol{A} = (0, Bx)$ we first calculate what is the size of the system so

that the peirels phases repeat themselves. Doing this will enable us to work with a magnetic unit cell that is periodic. For simplicity we will assume $\hbar = 1, e = 1$. That is, the magnetic flux of 2π is to be interpreted as one flux quantum. We have

$$\int \boldsymbol{A} \cdot \boldsymbol{dl} = \int (0, Bx) \cdot (dx, dy) = \int Bx \cdot dy = Bx(y_2 - y_1) \tag{4.5}$$

Then,$Bx(y_2 - y_1) = mBa^2$ where $m\epsilon 0, 1, 2, ...$ Integration is to be done over the path from i^{th} site to j^{th} site..We can associate a phase of $e^{\iota \int \boldsymbol{A} \cdot \boldsymbol{dl}}$ with each hopping. As we know that $B = \frac{\Phi}{A}$, we choose $\Phi = \frac{2\pi}{4}$ and the area of one plaquette is a^2. This gives $B = \frac{2\pi}{4a^2}$. Putting the values in the phase, we get $e^{\iota \frac{2\pi}{4a^2} ma^2}$. This gives the condition for m as $m = 4n, n = 1, 2, 3, ...$ if we want to repeat the values of Peirels phase. In other words, if we take 4 unit cells, we make a magnetic unit cell that has the required periodicity. We can see from above calculation that the Peirels phase and magnetic unit cell depends on the gauge chosen for $\boldsymbol{A}$.

Now for graphene, we follow a similar procedure. This time, we use symmetric Gauge for $\boldsymbol{A}$ i.e, $\boldsymbol{A} = \frac{B}{2}(-y, x)$. Here the situation is a bit more complicated. For the geometry considered in the figure 4.3, we will calculate the peirels phases that give the periodicity condition.

There are three types of nearest neighbour hoppings that are possible in Graphene, along the vectors that connect the neighbours of an atom. Our geometry extends in two directions that are given by translation of the lattice vectors $\boldsymbol{a_1}$and $\boldsymbol{a_2}$. We first calculate the peirels phases associated with vertical hoppings in $\boldsymbol{a_1}$ direction.

Area of one plaquette, $A = \frac{3\sqrt{3}}{2}a^2$. As the above case, magnetic flux passing through each plaquette is $\frac{2\pi}{4}$. So,

$$B = \frac{2\pi}{4}\frac{1}{A} = \frac{2\pi}{4}\frac{2}{3\sqrt{3}a^2}$$

.

$$\int \boldsymbol{A} \cdot \boldsymbol{dl} = \int \frac{B}{2}(-y, x) \cdot (dx, dy) = \frac{xaB}{2}$$

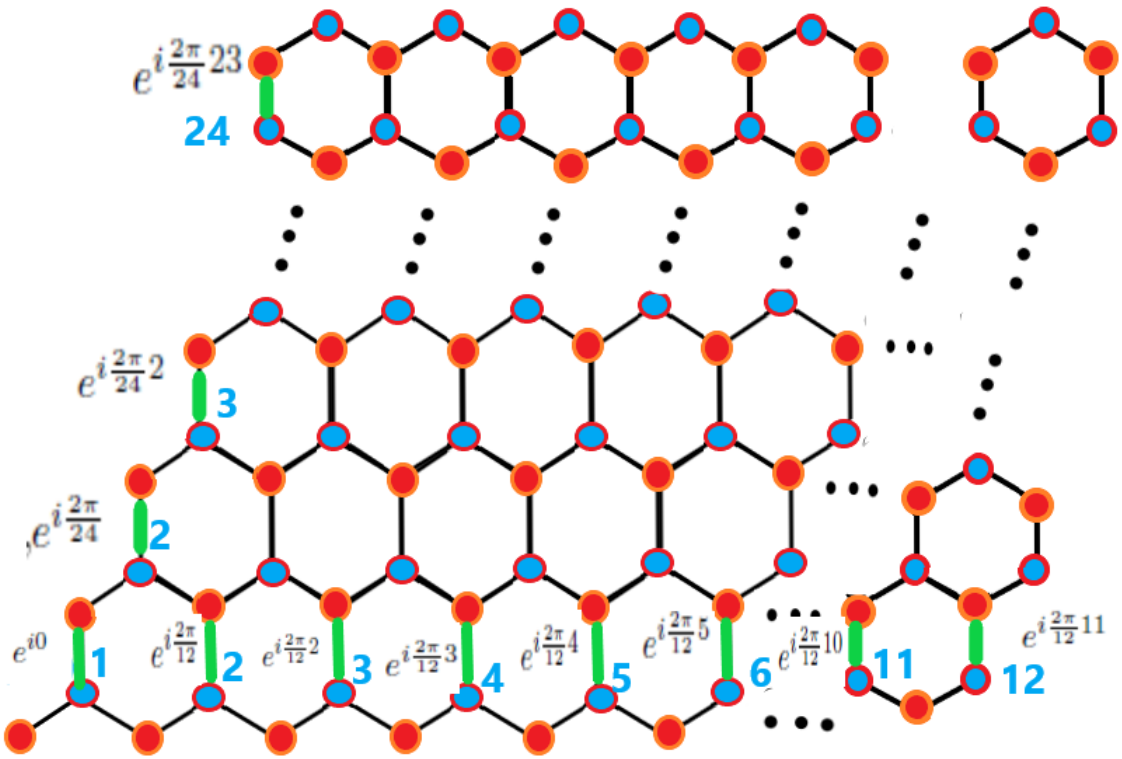

Figure 4.3: Graphene with origin fixed at first A atom and extended in both $\boldsymbol{a_1}$ and $\boldsymbol{a_2}$. Peirels phases are indicated along the green bonds. Blue atoms are A type and Red atoms are B type.

$x = ja\sqrt{3}$ in $\boldsymbol{a_1}$ direction. So,

$$\int \boldsymbol{A} \cdot \boldsymbol{dl} = \frac{ja^2\sqrt{3}}{2} B$$

This gives a Peirels phase of $e^{\iota\frac{2\pi}{12}j}$ where $j = 0, 1, 2...$ hence the condition for periodicity in $\boldsymbol{a_1}$ direction for vertical hoppings is $j = 12 * integer$.

The same calculation done for vertical hoppings in $\boldsymbol{a_2}$ direction will have $x = \frac{ma\sqrt{3}}{2}$. This gives $\int \boldsymbol{A} \cdot \boldsymbol{dl} = \frac{ma\sqrt{3}}{4} B$. So the periodicity condition is $m = 24 * integer$.

This procedure is repeated for hopping in the $\boldsymbol{\delta_2}$ and $\boldsymbol{\delta_3}$ directions. The least common multiple of all the above conditions will be considered to be the smallest size of the system

which is periodic. In our case, we find that 24 is the integer that is the LCM. So, we consider system size of 24×24 in our numerical calculations.

Chapter 5

Spectrum of Graphene in Hofstadter regime

We simulate a Monolayer Graphene of size 48×48 in $\boldsymbol{a_1}$ and $\boldsymbol{a_2}$ directions. We first insert through Peirels phases, $\frac{2\pi}{4}$ flux which is very large and hence, well in the Hofstadter regime. When we impose periodic boundary conditions in both directions, we will get the landau level spectrum. There are gaps between levels and landau levels are highly degenerate. The landau levels are not exactly flat. This is the difference we observe between Hofstadter model and continuum model.

We apply the periodic boundary conditions when we like to study the bulk properties of the system and apply open boundary conditions when we are interested in studying the edge states and it's effects. Periodic boundary conditions create a torous like geometry and in case of open boundary condition, we can get two types of edges namely: The zigzag edge and the Armchair edge which have very different transport properties. When we impose edge in one direction and form a ribbon geometry, we find some new states that are formed in the gaps between landau levels. These are called edge states. They can be identified in two ways pictorially. From a plot of Eigenvalues in which the points are coloured according to y expectation values of corresponding eigenvectors, states located on upper edge will have higher y expectation values and vice versa(figure 5.1). Or we can also plot Eigenvalues and colour according to the IPR's of corresponding wavefunctions(figure 5.2).

One curious case is that of a localized state that appears at the $E = 0$ level in the centre

of $n = 0$ landau level. This is different from other edge states because the others appear in the gaps between landau levels whereas, this state appears at the centre of landau level. This is protected by sublattice symmetry that occurs because Hamiltonian has

$$-t \sum_{A,B} {c_A}^{\dagger} c_B$$

term and it's Hermitian conjugate which under the operation that c_B goes to $-c_B$, the Hamiltonian changes from H to $-H$. This implies that,

$$[T, H]_+ = 0 \tag{5.1}$$

Then energy bands appear in pairs like kramers pairs. The two band have opposite velocities.

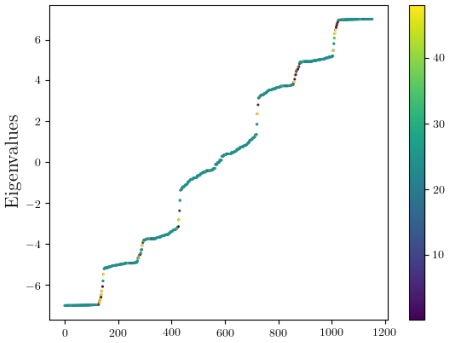

Figure 5.1: Monolayer Graphene in presence of $\frac{2\pi}{4}$ magnetic flux.Color bar indicates the y expectation value of the eigenvector corresponding to that eigenvalue.

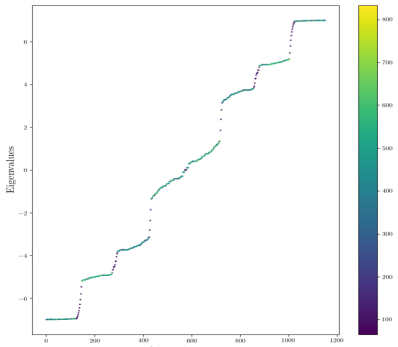

Figure 5.2: The Eigenvalues can also be coloured by IPR's of corresponding eigenvectors

We expect that the landau levels should be flatter if the flux inserted through each plaquette is reduced. That is what figure 5.3 confirms. The $n = 0$ landau level has twice the number of states than other levels as is shown by DOS calculation. Having a system which is not periodic will reduce the landau level degeneracy and create states in the gaps. Already according to Peirels argument, we have seen how to create a periodic system in magnetic field. If we do not take a system with the size given by that condition, we see some effects that are artefacts of small system size which is not desirable. From figure 5.4 we find that changing system size slightly from periodicity condition produces some states in the gaps and other unwanted effects. This happens because one plaquette will have a different flux passing through than all others.

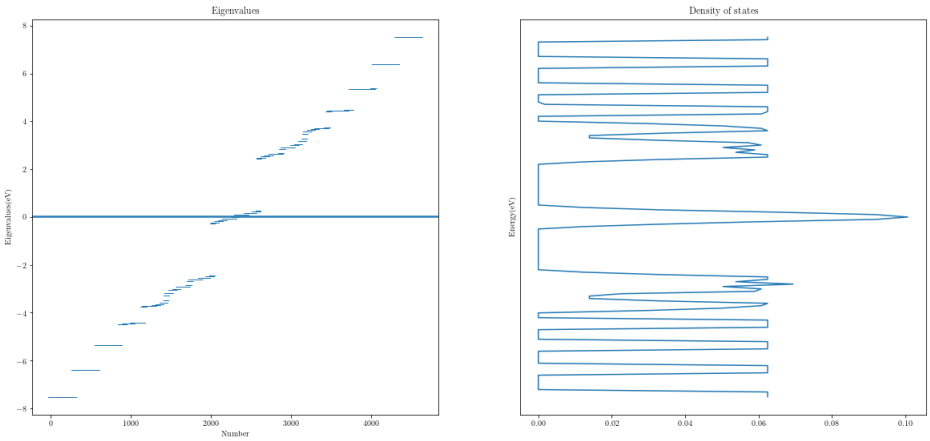

Figure 5.3: Landau Levels for a Graphene lattice with periodic boundary conditions of 48×48 size in presence of a magnetic flux of $\frac{2\pi}{8}$ and corresponding density of states simulated.

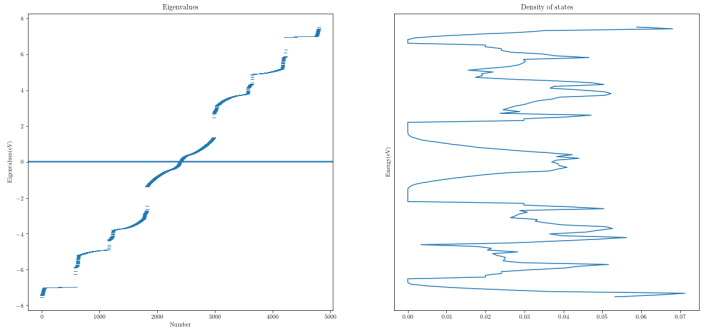

Figure 5.4: Landau Levels for a Graphene lattice of $49 * 49$ size in presence of a magnetic flux of $\frac{2\pi}{4}$ and corresponding density of states simulated.

Chapter 6

Impurities and Disorders in Graphene

Very rarely do we ever get a system which is impurity free. Impurity can appear in different ways like a random on-site potential or dislocation of an atom from lattice site or replacement of lattice atom with some other atom.

In case of random potentials, for convenience, we restrict the random potential to be uncorrelated at different spatial points. We employ numerical diagonalisation of the Hamiltonian because we cannot use perturbation theory techniques as landau levels are highly degenerate. We study two types of disorders namely on-site or diagonal disorder and bond disorder or off-diagonal disorder.

Consider a Hamiltonian

$$\boldsymbol{H} = \sum_i V_i c_i^\dagger c_i + \sum_{<i,j>} (t_{i,j} e^{i\theta_{i,j}} c_i^\dagger c_j + H.C) \tag{6.1}$$

The V_i correspond to on-site energies that we take to be random. It describes a potential disorder. The randomness in $t_{i,j}$ describe bond disorder. This disorder corresponds to randomness in the fermi velocity v_F and B. With this connection, the Fermi velocity becomes position dependent. The fluctuations of the phase $\theta_{i,j}$ correspond to a magnetic field that is position dependent.

Recent studies on the shape of broadened $n = 0$ landau level shows two features that are a bit unusual. First, the $n = 0$ landau level shape is a gaussian with shallow minimum at

the centre of the level and it has very narrow peak on top of this minimum.

The theoretical description of bond disorder in momentum space was given by T.Ando[9]. The monolayer Hamiltonian, as we already know from previous sections is:

$$\mathbf{H}_0 = \hbar v_F \begin{pmatrix} \vec{\sigma}\cdot\vec{q} & 0 \\ 0 & -\vec{\sigma^\star}\cdot\vec{q} \end{pmatrix} = \hbar v_F \begin{pmatrix} 0 & q_x - \imath q_y & 0 & 0 \\ q_x + \imath q_y & 0 & 0 & 0 \\ 0 & 0 & 0 & -q_x - \imath q_y \\ 0 & 0 & -q_x + \imath q_y & 0 \end{pmatrix}$$

and

$$U_i(\boldsymbol{r}) = \begin{pmatrix} 0 & z_A^\star z_B & 0 & z_A^\star z_B^{'} \\ z_B^\star z_A & 0 & z_B^\star z_A^{'} & 0 \\ 0 & z_A^{\star'} z_B & 0 & z_A^{'\star} z_B^{'} \\ z_B^{'\star} z_A & 0 & z_B^{'\star} z_A^{'} & 0 \end{pmatrix} u(\mathbf{r} - \mathbf{r_i}) \tag{6.2}$$

where $z_s = e^{\imath \mathbf{K}\cdot\mathbf{R_s}}$ and $z_s^{'} = e^{\imath \mathbf{K}^{'}\cdot\mathbf{R_s}}$, s=A,B. $u(\mathbf{r} - \mathbf{r_i})$ is the change in hopping matrix element. $\sum_i U_i$ is a generic bond disorder. A scatterer located on one sublattice A at a position $\mathbf{r_A}$ can be written as:

$$U(\boldsymbol{r}) = \begin{pmatrix} 1 & 0 & z_A^\star z_A^{'} & 0 \\ 0 & 0 & 0 & 0 \\ z_A^{'\star} z_A & 0 & 1 & 0 \\ 0 & 0 & 0 & 0 \end{pmatrix} u\delta(\mathbf{r} - \mathbf{r_A}) \tag{6.3}$$

For these disorders and k-space Hamiltonian, we can solve in the self consistent Born Approximation when the range and strength of disorder is small so that inter landau level mixing is neglected.The conductivity is obtained by kubo formula. If the disorder is long ranged, then the DOS is obtained in eikonal approximation.For lower landau levels and uncorrelated disorder, the problem is that there is no small parameter so neither approximation helps.

Chapter 7

Flux threading argument

Laughlin first gave an argument which explains the existance of edge modes and connected it to the Hall conductance[6]. In his argument, he considers a 2D square lattice system which is periodic in y-direction and has edges in x-direction. Then he adds an additional phase in the y-direction hoppings. This changes the k_y of the system to $k_y + \frac{2\pi\Phi}{L_y}$. If we connect the edges to leads and create a potential difference V and measure the current in y direction which is the Hall effect setup, the current operator can be obtained from the Hamiltonian by:

$$j_y = \frac{\partial H}{\partial k_y} \tag{7.1}$$

The expectation value of this current in ground state is called Byers-yang formula.

$$< j_y >= \frac{\partial E}{\partial \Phi} \tag{7.2}$$

If flux threaded is changed adiabatically from $\Phi = 0$ to $\Phi = 2\pi$, we know that the Hamiltonian is invariant under this process. The individual energy levels or eigenfunctions of the Hamiltonian need not stay constant. They can morph into each other. This phenomenon is called spectral flow. This is a critical part to understand Quantum hall effect. When one flux quantum is inserted, all the energy bands that crosses fermi level and on one edge, will have one more filled momenta and on the other edge, one less filled momenta. As there is a potential difference between two edges, this means that the energy provided by flux insertion

is equal to the energy change of ν charge carriers in Potential V. $\Delta E = \nu V e$ ν is the number of bands that cross fermi level. The conductivity then becomes

$$\sigma_{xy} = \frac{I_y}{V_x} = (\frac{\nu e^2 V_x}{h})(\frac{1}{V_x}) = \nu \frac{e^2}{h} \tag{7.3}$$

Therefore, the number of edge modes is directly proportional to the Hall conductance. We can count the total number of edge modes from band structure calculation and compute Hall conductance.

In our numerical computations, we have the lattice with zig-zag edges and the system is like a parallelogram which means even if we put periodic boundary conditions in one of the directions and make it a ribbon geometry, k_x or k_y cannot be used in momentum space calculations. The reciprocal lattice vectors do not form an orthogonal basis. Unless specified otherwise, we will consider periodic boundary condition in $\mathbf{a_2}$ direction and edges in $\mathbf{a_1}$ direction. According to Laughlin flux argument, we will introduce flux inserted as a phase for hopping perpendicular to the periodic direction($\mathbf{a_2}$). From the figure7.1 of our geometry this corresponds to hopping in the $\delta_\mathbf{2}$ direction.

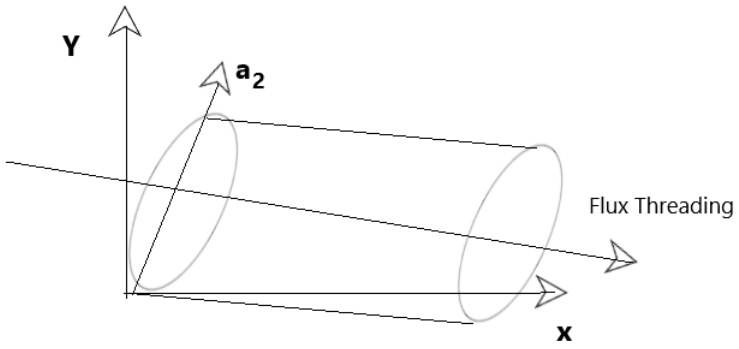

Figure 7.1: Laughlin Flux cylinder

Let's consider the situation in which we have a lattice which has periodic boundary conditions in y direction and has edges in x direction. Now let's add random impurities at every lattice site. This system is clearly not translation invariant. We would like to study the edge modes behaviour and dispersion relation in this system. Towards this goal we create multiple copies of this disordered system and place them next to each other like in the Figure 7.2. Now this system forms a lattice along x-direction. We can associate a momentum space

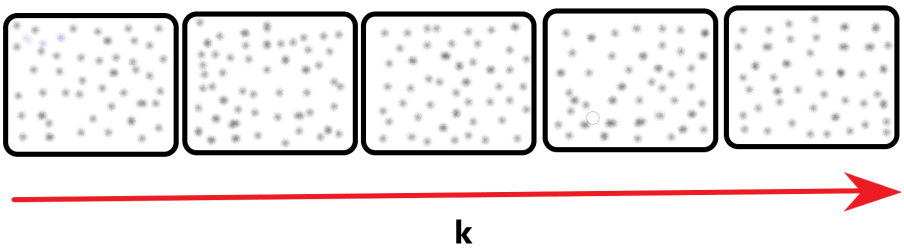

Figure 7.2: Multiple copies of a disordered system forming a 1D lattice

with lattice and call the parameter k just like in 1D lattice. To find the band structure of this system, we can take a unit cell which in our case is the lattice we want to find the band dispersion for and the flux threading we considered earlier can be mapped to the momentum k and then we can use Φ to find out the dispersion and other aspects of band structure. This is the technique we employ to obtain a "band structure" for the disordered systems. As

$$E = -\frac{\partial \Phi}{\partial t} \tag{7.4}$$

By slowly inserting the flux, we are creating an electric field along with the existing radial magnetic field. This setup gives the Quantum hall regime. We will show that Edge modes undergo spectral flow in the presence of electric field and Bulk modes do not.

Chapter 8

Results for Band structure in Monolayer Graphene

As was discussed in the previous chapters about the idea of flux threading serving as wavenumber and enabling us to find the band structure of systems, in this section, we implement that idea numerically in case of Monolayer Graphene. Including all the different types of disorders in an analytical calculation becomes a difficult problem to keep track of. So, we shall stick to numerical computations.

8.0.1 Pure Graphene in Ribbon Geometry

The first case we consider for the calculation of band structure is that of pure monolayer graphene with a magnetic flux $\frac{2\pi}{4}$ through each plaquette. The $\boldsymbol{a_2}$ direction is taken to be periodic. The flux threading increases from $\Phi = 0$ to $\Phi = 2\pi$. The energies are plotted on y-axis. The edge modes in Graphene as we have already discussed, are chiral. Their direction of propagation is opposite on the two edges. They contribute in conduction of current in Quantum Hall state.

The figure 8.2 shows the band structure for pure Graphene. We can see the bulk states forming the bands and edge states present in the band gaps.These edge states can travel from one band to another thereby forming a channel for conducting current. In a sense, edge states are more pure states than bulk states because, they have contribution only from

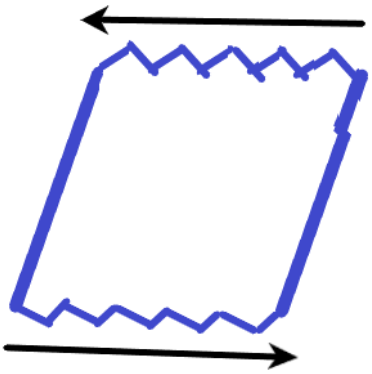

Figure 8.1: Cartoon of the geometry considered. The rigged zig-zag type edges in x direction ($\mathbf{a_1}$)are the edges and in the $\mathbf{a_2}$ direction(straight lines in figure) system is periodic. Directions of edge modes propagation are shown.

atoms on the edge whereas,the bulk states have contribution from all the bulk atoms.

To understand which edge mode comes from which edge, we can use color coding of y- expectation values of eigenfunctions. The edge mode travelling near $y = minimum$ (one edge of the ribbon)can be distinguished from edge mode at $y = maximum$(Other edge of the ribbon). This is an useful identification to keep track of directionality of edge modes. From figure 8.3, we find that edge mode localized near $y = max$ flows in the direction of increasing energy and the edge mode localized near $y = min$ flows in the direction of decreasing energy. Bulk states are spread everywhere in the bulk and hence y-expectation values for them is about half the ribbon width. Bulk states do not show spectral flow. After a flux insertion of 2π, they come back to the original energy state but the edge modes can be seen changing in energy and travelling to different bands. The whole band structure clearly has flat bands with edge modes in between bands.

We know that Graphene has sublattice degree of freedom. We can probe the projection of eigenfunctions on A sublattice and B sublattice to see if the system has different properties on different sublattice. In the case of pure Monolayer Graphene,we see that the eigenfunctions are equally spread on both sublattices which implies the sublattice symmetry. If an energy E is present, then energy $-E$ is also present.

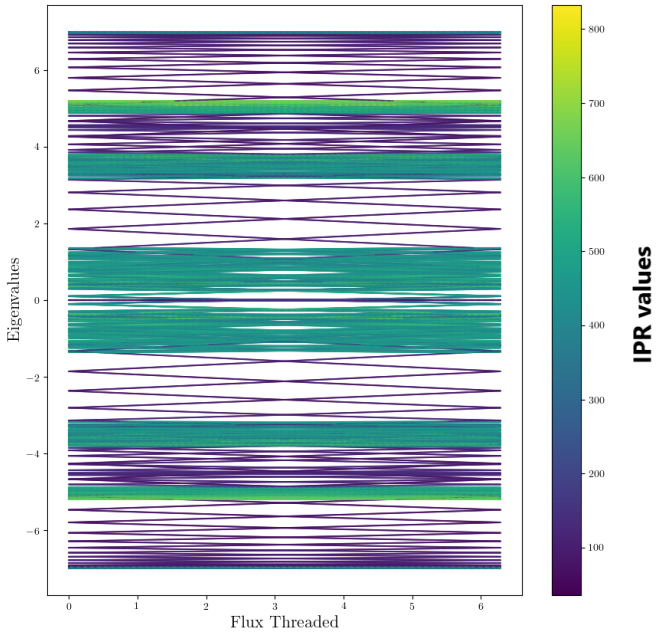

Figure 8.2: Band structure for monolayer graphene in presence of radial magnetic flux and flux threading. The colorbar shows the IPR values. It can be recalled that edge states have smaller IPR than bulk states.

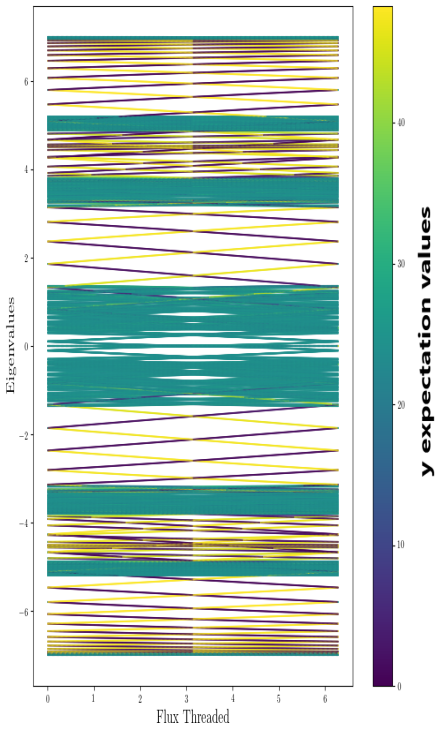

Figure 8.3: Band structure for Pure Monolayer graphene color coded by y-expectation values of eigenfunctions.

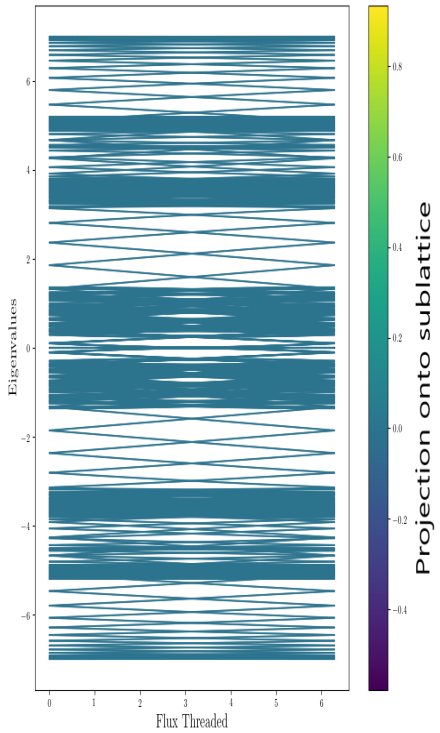

Figure 8.4: Projection onto A and B sublattice. The most negative values corresponds to wavefunctions localized on B sublattice and vice-versa

8.0.2 Graphene Ribbon with random impurities at each site

When we include random impurities in the range of energies 0 eV to 0.5eV on each lattice site, we do not see any qualitative difference in the spectrum from that of figure8.3 other than slight changes in energy levels.This implies that random impurities were not able to localize and destroy edge modes.

8.0.3 Coupling between two atoms within the Bulk

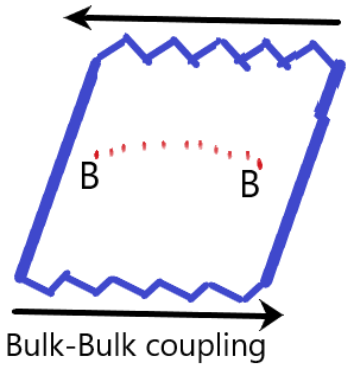

Figure 8.5: Cartoon for the Bulk-Bulk scattering. Two B atoms in the bulk have shown to be coupled.

Next we include random impurities and a scattering between two B type atoms within the bulk. The scattering strength is 2eV which is very strong coupling between the atoms. When we, in ribbon geometry, couple two atoms deep within the bulk, and have no edge coupling, we expect that edge modes continue to propagate unaltered. This intuition is correct. The figure8.6 shows no gap opening. There is an existence of an energy level that starts from a bulk band and flows back to the same bulk band. It is the energy levels of the system of the two coupled atoms in the bulk. The coupling is very strong compared to other energy terms in the Hamiltonian. So, for those states, our system is a perturbation instead of their coupling being perturbation to our system. Their energy level happens to be in the band gap.The y expectation value for that state shows that the state is strongly localized between the two atoms and not present at the edge.Projection onto the sublattice shows that the state is solely on B sublattice.

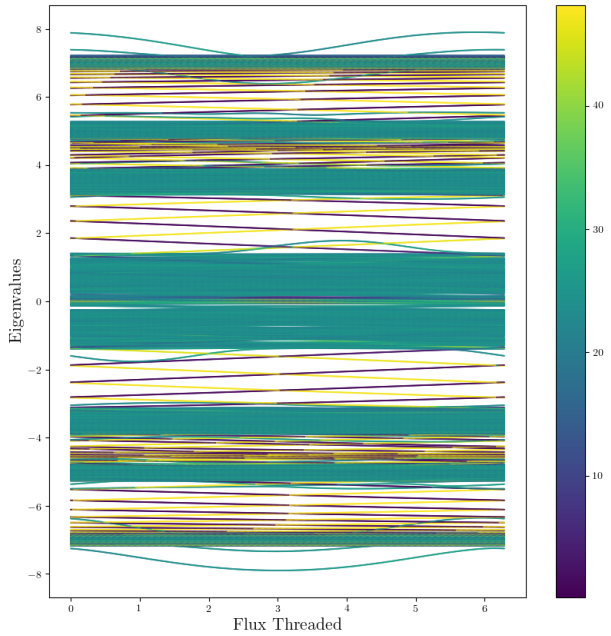

Figure 8.6: Band structure for Graphene with only Bulk-Bulk coupling. Colour represents the y expectation values of eigenvalues.

8.0.4 Coupling between two edge modes

Consider the figure8.7. In our simulations, the upper edge has A atoms on the edge and the lower edge has B atoms. When we insert a magnetic flux through this system, the two edge modes will be counter propagating. In other words, the chirality of two modes are opposite. When a scattering between two edges is established, now there is a chance for two chiral modes to couple and create a hybrid state in which the chirality of both of them is lost. Our system is in cylindrical geometry. When coupling between two edges are introduced it is like morphing the cylindrical geometry into a torus geometry which has no edges. In that case, the edge modes couple and a band gap opens up. This can be established by finding the y expectation values that tell us that edge mode on one edge no longer continues to be separate but hybridises with the other edge mode.

Figure8.8 shows the band structure. Opening of the band gap means that the edge modes no longer connect two bulk bands. This means that current flowing on the edge

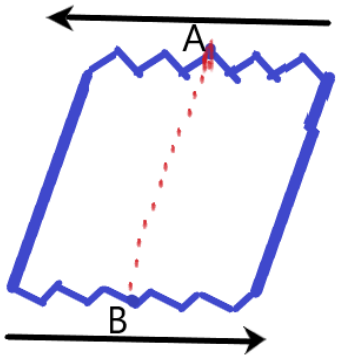

Figure 8.7: Cartoon for the edge-edge scattering. The lower edge has B type atom and upper edge has A type atom. Chiralities of modes are opposite.

now encounters resistance. It is no longer true that all the charges put on one end of the edge travels to the other end of the edge without encountering resistance. They could get backscattered as well. All the opposite moving edge modes pairs get gapped in this case.

Consider that pure Graphene Hamiltonian is H_0. The impurities can be considered to form a perturbation matrix H_{imp}. Now, we focus on one of the band gaps. Close to the centre of brillouin zone, consider two counter propagating edge modes. Let Ψ_1 and Ψ_2 be the eigenvectors at that point on the two edge modes respectively. Now,consider the matrix:

$$\begin{pmatrix} <\Psi_1|H_1|\Psi_1> & <\Psi_1|H_1|\Psi_2> \\ <\Psi_2|H_1|\Psi_1> & <\Psi_2|H_1|\Psi_2> \end{pmatrix} \tag{8.1}$$

The eigenvalues of this matrix will decide what happens when two states have same energy at a point. When the off diagonal terms are zero, we see that the energy eigenvalues will be $\pm E$ (say). When the $<\Psi_2|H_1|\Psi_1>$ and $<\Psi_2|H_1|\Psi_2>$ both give the same value, we will be left with a degenerate solution. But if the off diagonal terms were not zero, we trivially see that this degeneracy is lifted. This is the phenomenon of avoided level crossing. The off diagonal elements are the couplings we are introducing between edges. That means, the energies of two counter propagating modes can never cross. Hence we see a band gap opening and the system becomes an insulator. In the pure graphene case considered earlier, we notice that off diagonal terms are zero. Hence, there is no band gap opening in that case.

The band gap width depends on two factors: 1. The number of scatterers present 2. The strength of scattering. Stronger scatterers open larger band gap. This is intuitive that the matrix elements in that case will get larger contribution from scatterers which happen to be the off diagonal terms.

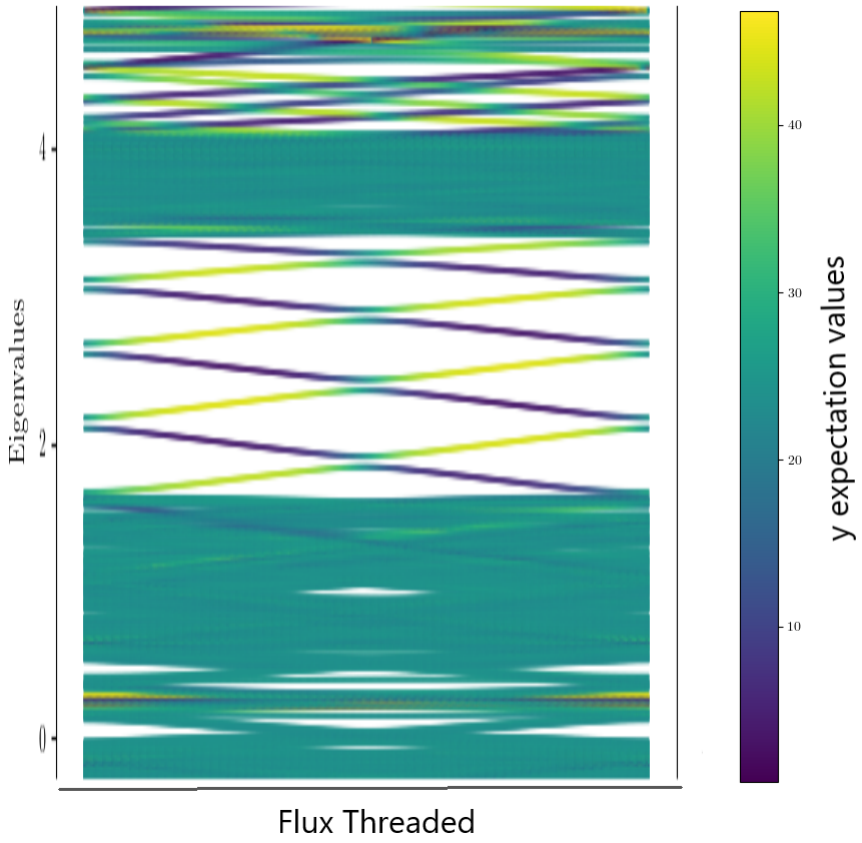

Figure 8.8: Zoomed in version of band structure for edge-edge coupling. We can see edge modes gapping out.

Chapter 9

Results for Band structure in Bilayer Graphene

In this thesis, we consider scattering problem in Bilayer graphene in IQHE states. The lattice termination can be of different types like zig-zag edge,armchair edge,braided edge etc. They all have different boundary conditions and hence different spectrum. Our work is focussed on zig-zag edges. We can have a Bulk-Bulk scattering between two atoms within the bulk. We can have A-B coupling, A-A coupling,B-B coupling, Edge-Edge scattering. Interlayer coupling,tuning of chemical potential,changing of magnetic flux in the layers etc. We will consider interlayer couplings here. Intralayer couplings can be thought of a cases similar to two copies of Monolayers. So, not much new physics can be learnt from it. We exclusively consider AB stacked Bernal Graphene in this thesis because it is the most commonly occurring and form of Bilayer Graphene.

9.0.1 Coupling through dimer bonds

Theoretical models and experimental results have shown that Bilayer graphene in Bernal stacking has A2 atoms on top of B1 atoms and there is a coupling between the two type of atoms with a hopping matrix element of -0.38 eV. The other hopping terms like next nearest neighbour terms are all found to be negligible. First, we will find the band structure for pure Bilayer Graphene in ribbon geometry when magnetic flux is $\frac{2\pi}{4}$ through each plaquette in

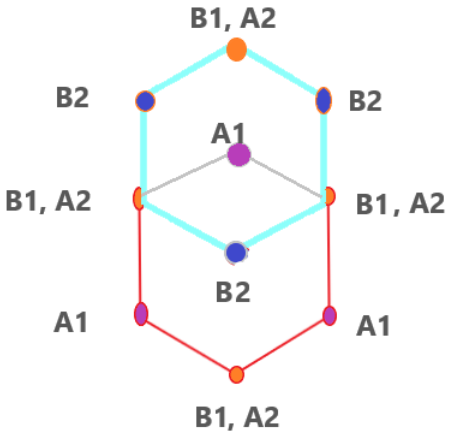

Figure 9.1: Bernal Stacking A2 atoms on top of B1 atoms and coupling between all A2 atoms with corresponding B1 atoms.

both layers and direction of magnetic field is also in $+z$ direction on both layers.

First we find that there are eight edge modes in the band gap closest to zero energy. There is no zero energy gapless mode that we had seen for Monolayer case. Though the B1-A2 coupling at all the sites are present, they do not open a band gap. They will all be bulk -bulk coupling because on the edges, there are no B1-A2 couplings. This shows how robust the edge modes are in Graphene. As there are no impurities present,excluding the interlayer couplings, the two layers are similar. This fact is to be kept in mind while doing numerical simulations as the programme that diagonalizes the Hamiltonian, when confronted with two eigenfunctions which are same on two layers, gives a linear combination of those two eigenvectors. So, in Bilayer case, identifying y expectation values and the projection of eigenfunctions on two layers are not indisputable and unique as was for Monolayer.

For Bilayer Graphene, we can also use the information of projection of wavefunctions onto two layers and extract which states are localized on just one layer and which ones have overlap on both layers.

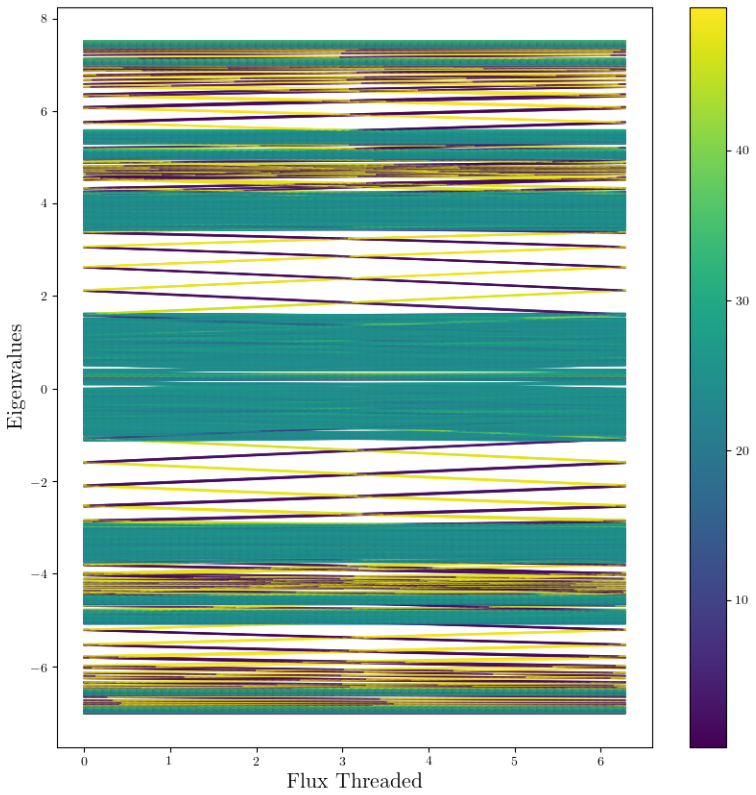

Figure 9.2: Spectrum when there is no coupling between edges but all A2 atoms coupled to B1 atoms. Colorbar shows y expectation values.

9.0.2 Co propagating modes and scattering between edges

Consider the situation in figure 9.3 When magnetic flux is in the same direction on both layers, no interlayer coupling other than edge-edge coupling exist, we expect that the edge modes remain robust as they have same chirality. The question may arise why we should expect that there be no coupling and thereby no gapping of edge modes. There is a classical way of looking at this from the point of view of cyclotron orbits. When an impurity is present such that it scatters between two edge modes, we can think of that as creating a potential around which electron forms a cyclotron orbit. It is in clockwise direction because of direction of perpendicular magnetic field. When the two co poropagating edge modes are coupled, due to chirality of edge modes, electron cannot traverse a clockwise cyclotron orbit

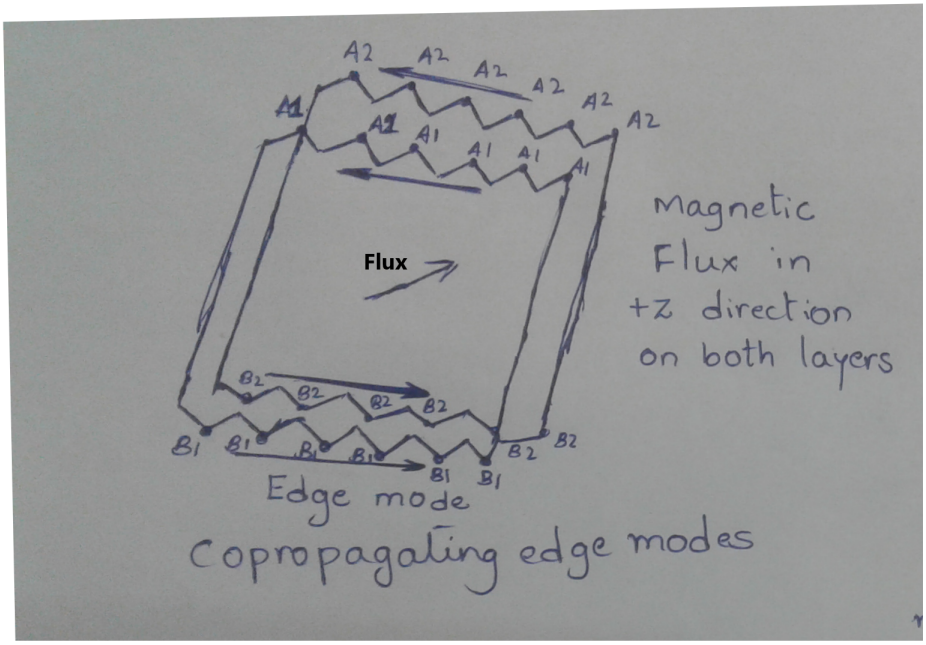

Figure 9.3: Cartoon of edges and periodic direction. Two layers sown as L1 and L2. Magnetic flux is in the same direction on both layers.

which means that even though we add scatterers coupling two co propagating edge modes,the electron on one edge mode just avoids and wades through that impurity and just continues to propagate in the same direction. In the figure9.4, that is exactly what we find. The edge modes continue to propagate in their direction when edge-edge coupling is introduced.

Including interlayer coupling like A2 and B1 atoms as in the case of real Bilayer Graphene, we do not see any noticeable new features in the spectrum that the number of edge modes remain same and thereby hall conductivity does not change. In the same way,coupling between an edge atom on one layer and an atom close to the edge on the other layer but not on the edge has no effect on edge modes. Strength of scattering has no effect on the spectrum either. Even if coupling between edge atoms is favourable for hopping, chirality forbids gapping of edge modes.

When a strong scattering between two bulk atoms one in each layer is added, just like Monolayer case, the strong coupling will not affect edge modes. When no random impurities are present,the bulk spectrum will be symmetric around $\Phi = \pi$ and the edge modes undergo

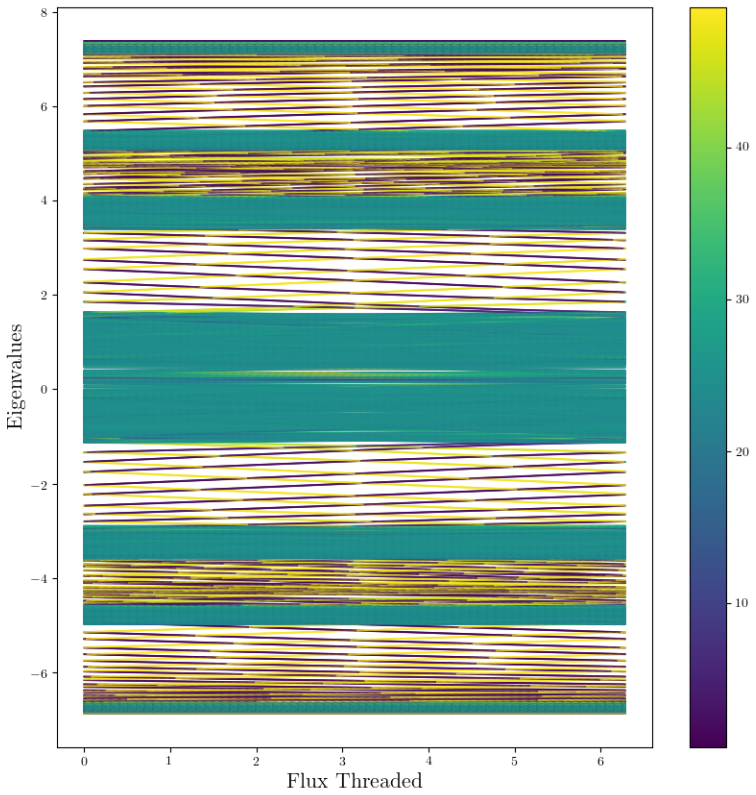

Figure 9.4: Co propagating modes coupled. Does not gap out the edge modes. Colours are the y expectation values of eigenvalues.

spectral flow.

9.0.3 Strong coupling of all A2 and B1 atoms

When the interlayer dimer bonds coupling is introduced, and magnetic flux is in the same direction in both layers, With the gradual increase in the strength of dimer bonds interlayer coupling, we see that bulk energy bands reduce in width and more band gaps are formed. This can be explained by noticing that, by creating a B1-A2 coupling, we are breaking the intralayer sublattice symmetry in the sense that A1 atoms and B1 atoms were equivalent before and now the B1 atom has coupling to A2 atom and vice versa. This makes A1 atoms

different from B1 atoms. Due to this, bulk bands split creating edge modes in the band gaps. The strength of coupling is also very important in determining the split in bulk bands as we notice that splitting is not very evident when coupling strength was kept at -0.4eV but becomes more prominent as strength increases. The figure 9.5 is for the case of coupling strength of -2.0eV. Compare this with no coupling between A2-B1 atoms.

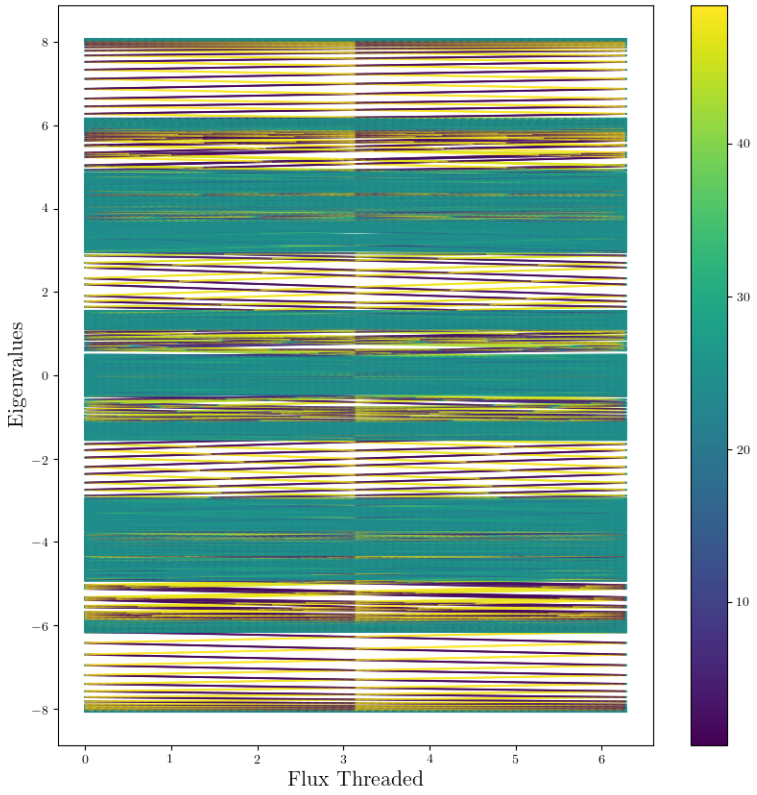

Figure 9.5: Very strong Dimer bond coupling. No gapping of edge modes but bulk bands split.

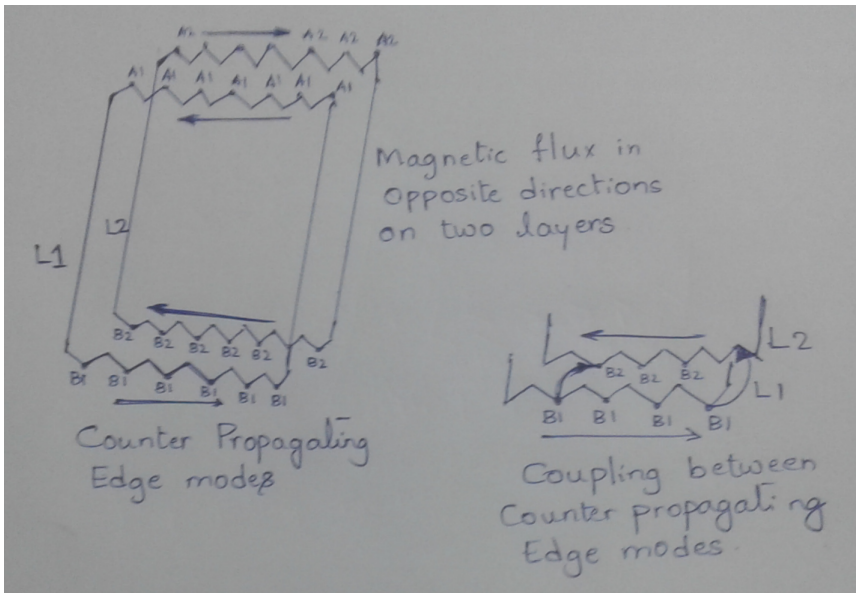

Figure 9.6: Counter propagating modes.When magnetic field in both layers are in opposite direction.

9.1 Magnetic flux on both layers in opposite direction

In this case, we put the magnetic flux on both the layers in opposite direction.We include random impurities as well. The edge modes are counter propagating. As we have not yet included the coupling between edges, the edge modes are degenerate and no gapping occurs. The random impurities are not strong enough to change the eigenvectors considerably which makes the programme to give a linear combination of edge modes reflected in y expectation colouring. We cannot distinguish between different edges because of this reason.

9.1.1 Bilayer Counter propagating edge modes coupling

Consider a Bernal stacked graphene with magnetic flux on the two layers pointing in opposite directions($+z$ and $-z$).As edge mode chirality is dependent on direction of magnetic flux, if there are edges on the same side in both the layers, the edge modes they harbour will have opposite chirality. In this scenario, if we had a coupling between two edges, we can expect a band gap opening through hybridization of edge modes which occurs because of avoided level crossing as was explained in last chapter. In our cyclotron orbit picture from previous sections,we can explain this case by noticing that a clockwise cyclotron orbit is possible to

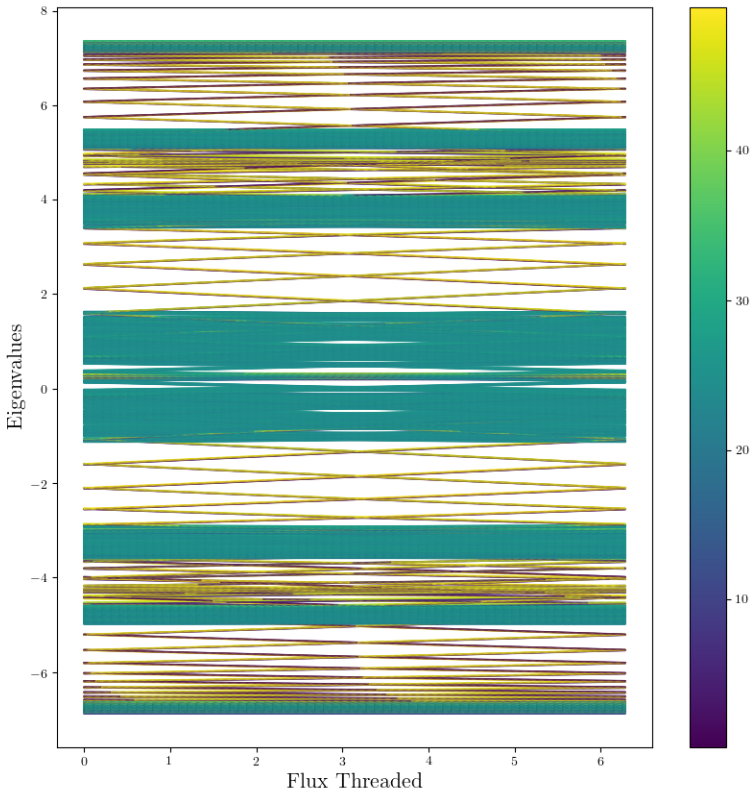

Figure 9.7: Magnetic flux on both the layers are in opposite direction. Random impurities of small strength included. y expectation values are unreliable.

be executed by the electron and such a coupling is not forbidden by chirality.

The fact that the edge modes on both layers are hybridizing can be substantiated even more by plotting the spectrum with colouring eigenstates based on projection onto two layers. An edge mode starting on one layer will hybridize with the edge mode from other layer and projection of eigenstates onto the layers will change.

Again, if we include scattering between edge modes along with bulk-bulk coupling, we see that band gap at different energy levels are different like it was in Monolayer case.

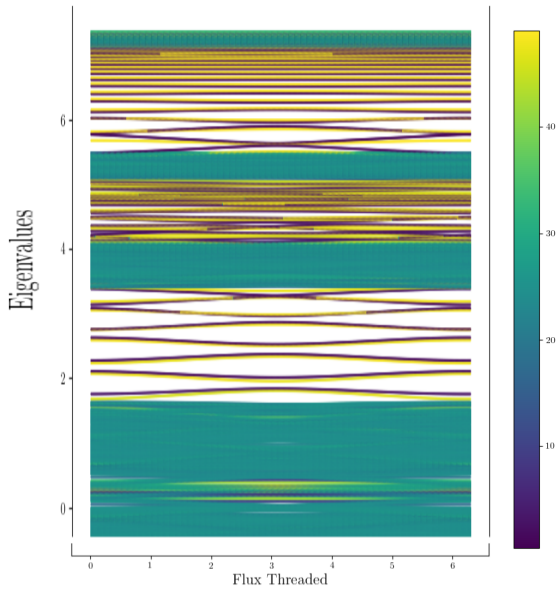

Figure 9.8: Zoomed in figure of spectrum of counter propagating modes coupling.The edge modes hybridize and gap out. Colours represent y expectation values of eigenvalues.

9.2 Chemical potential difference between layers

This case is very much of practical interest. It has been noticed experimentally in a remarkable discovery that in Bilayer Graphene, we can tune band gap by applying a perpendicular electric field. The electric field can be incorporated into our hopping Hamiltonian as chemical potential difference between layers which appear as diagonal elements in the Hamiltonian.

Consider a scenario when two layers are decoupled(meaning, there is no interlayer hopping). Then, it is like two copies of independent monolayers. The spectrum will be the same as that of monolayer graphene if magnetic flux is in the same direction on both layers. We have already seen the landau level structure in monolayer graphene in figure **??** Now, we shift all the energies of one layer by a constant value such that the new landau level energies of the shifted layer coincides with that of the next landau level of the other layer. If we impose Ribbon geometry, edge states appear between the landau levels. But the number of edge states on both the layers will be different for a given energy window as the spectrum of one layer has been shifted. In this case, when we introduce coupling between these two layers, the edge states in (say) first band gap of one layer will couple with the second (say) band gap

of the next layer. This is because of the fact that scattering matrix elements have terms that favour scattering between two states of comparable energies and exponentially suppress the scattering between two states of different energies as they require large momentum transfer.

The number of edge modes are different at different band gaps. Let's say in a band gap there are n modes in one layer and in the same gap, m modes are there in the other layer after we shift the chemical potential of that layer. If magnetic flux on both layers are in opposite in direction, from previous discussions, we expect all the opposite chirality edge modes to gap out in pairs when a coupling between them is introduced. Difference here is that equal number of edge modes are not travelling in opposite directions. So, some edge modes will not be fully gapped out and survive. They form what are called as gapless edge modes that flow from one band to other when flux threaded changes from 0 to 2π. We can write a simple formula for number of gapless edge modes g in a band gap,as,

$$g = n - m \tag{9.1}$$

where n and m are number of edge modes contributed by each layer in that band gap. So, by this method, we can somewhat tune the hall conductance of graphene bilayer by shifting relative potential between layers. Comparing the figure 9.9 with that of chemical potential being zero (figure 9.8), we notice less number of edge modes.

The projection onto two layers shows that each bulk state is exclusively localized on one of the layers and edge modes are coupled having equal overlap on both layers.

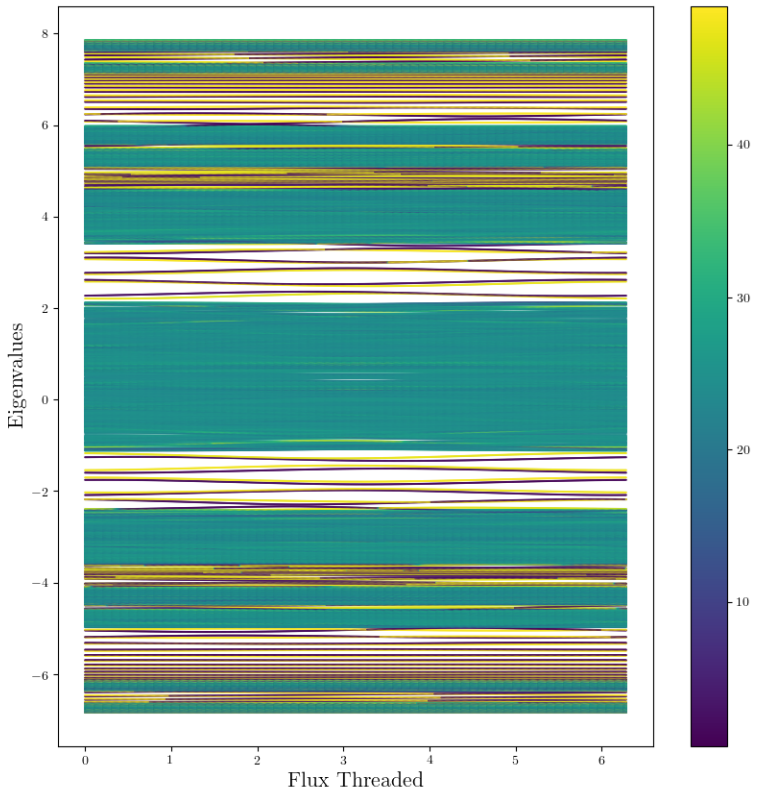

Figure 9.9: Bandstructure when a chemical potential of one of the layers is changed by 0.2 eV.

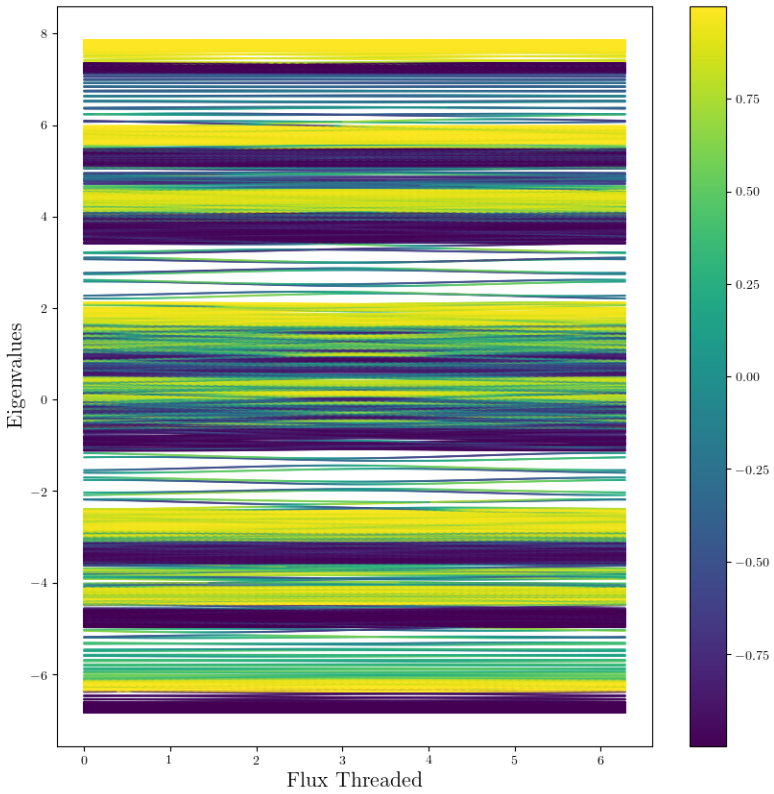

Figure 9.10: Bandstructure when a chemical potential of one of the layers is changed by 0.2 eV. The colouring is related the projection onto each layers. The most negative values denoting states which are fully localized in layer 2 and most positive values denoting states exclusively localized in layer 1.

Chapter 10

Conclusion

In this thesis we studied analytical description of monolayer graphene in the continuum limit which has Dirac spectrum with linear dispersion and relativistic landau levels. Then we studied Bilayer Graphene analytically and found that it has parabolic bands and quadratic dispersion. Then we discussed Hofstadter model of honeycomb lattice because continuum model regime is applicable only under small magnetic fields and it is numerically costly to implement the continuum model. The Honeycomb lattice was used in the study instead of square lattice because of richer phase space it provides with valley degree of freedom and is the lattice type to which graphene belongs which is a material with many properties that are of academic and research interest. The spectra for landau levels of Graphene in Hofstadter model was studied numerically. Solving Harper equation for Honeycomb lattice, the fractal spectrum Hofstadter Butterfly is observed.

Using the bulk edge correspondence established by Laughlin gauge argument and connecting flux threading to hall conductance by Bayers-Yang formula, we obtained band structures for monolayer and bilayer graphene with disorder in the IQHE regime and qualitatively studied their conductivity. We numerically studied the properties of edge modes and their stability in the integer quantum hall regime. The edge modes were found to be chiral and very robust in the presence of magnetic field under all the cases where coupling did not respect the chirality condition that edge modes undergo change only when we couple two counter propagating edge modes and the robustness was lost when we coupled counter propagating edge modes. We tracked this change with the edge bandgap opening. The chirality was

tracked with position operator expectation values, Inverse participation ratios, projection of wavefunction onto sublattice and onto the layers(in case of bilayer). Multiple scenarios like scattering between edge modes, scattering within sublattice, effect of direction of magnetic flux,effect of strength of scattering potential, interlayer coupling,tuning of chemical potential etc. were worked out. We established that edge modes remained stable and back scattering is absent under multiple scenarios(that don't respect chirality condition) which in other conventional materials would have led to strong localization of edge modes.

An immediate next goal could be to study the Bilayer Graphene with no interlayer coupling but strong repulsive interaction between two atoms belonging to different layers at just one point. This problem will have a large Hilbert space as it involves interaction.

The outlook is to ultimately study the electron-electron interaction problem of Fractional quantum Hall regime for Bilayer graphene and also it's coupling with superconducting qubits and the case of twisted bilayer graphene. These problems are not tractable analytically. So, a numerical calculation will be necessary. In this work, we have identified and worked with the physical parameters and numerical tools upon tracking which, information about the phase and state of the system can be revealed. Using these numerical tools in the more complicated cases of FQHE coupled edge theory will prove to be quite useful.

Bibliography

[1] Cristina Bena. Effect of a single localized impurity on the local density of states in monolayer and bilayer graphene. *Physical review letters*, 100(7):076601, 2008.

[2] KI Bolotin. Electronic transport in graphene: towards high mobility. In *Graphene*, pages 199–227. Elsevier, 2014.

[3] Vladimir I Fal'Ko. Electronic properties and the quantum hall effect in bilayer graphene. *Philosophical Transactions of the Royal Society A: Mathematical, Physical and Engineering Sciences*, 366(1863):205–219, 2007.

[4] Mark O Goerbig, Roderich Moessner, and Benoît Douçot. Electron interactions in graphene in a strong magnetic field. *Physical Review B*, 74(16):161407, 2006.

[5] MO Goerbig. Electronic properties of graphene in a strong magnetic field. *Reviews of Modern Physics*, 83(4):1193, 2011.

[6] Bertrand I Halperin. Quantized hall conductance, current-carrying edge states, and the existence of extended states in a two-dimensional disordered potential. *Physical Review B*, 25(4):2185, 1982.

[7] Yasuhiro Hatsugai, Takahiro Fukui, and Hideo Aoki. Topological analysis of the quantum hall effect in graphene: Dirac-fermi transition across van hove singularities and edge versus bulk quantum numbers. *Physical review B*, 74(20):205414, 2006.

[8] Dong-Keun Ki, Sanghyun Jo, and Hu-Jong Lee. Observation of chiral quantum-hall edge states in graphene. *Applied Physics Letters*, 94(16):162113, 2009.

[9] Mikito Koshino and Tsuneya Ando. Splitting of the quantum hall transition in disordered graphenes. *Physical Review B*, 75(3):033412, 2007.

[10] Viktor Krueckl and Tobias Kramer. Revivals of quantum wave packets in graphene. *New Journal of Physics*, 11(9):093010, 2009.

[11] Rupali Kundu. Tight-binding parameters for graphene. *Modern Physics Letters B*, 25(03):163–173, 2011.

[12] RB Laughlin. Levitation of extended-state bands in a strong magnetic field. *Physical review letters*, 52(25):2304, 1984.

[13] Edward McCann and Vladimir I Fal'ko. Landau-level degeneracy and quantum hall effect in a graphite bilayer. *Physical Review Letters*, 96(8):086805, 2006.

[14] Edward McCann and Mikito Koshino. The electronic properties of bilayer graphene. *Reports on Progress in Physics*, 76(5):056503, 2013.

[15] Sabyasachi Nag, Arti Garg, and TV Ramakrishnan. Nature of single-particle states in disordered graphene. *Physical Review B*, 93(23):235426, 2016.

[16] Norbert Nemec and Gianaurelio Cuniberti. Hofstadter butterflies of bilayer graphene. *Physical Review B*, 75(20):201404, 2007.

[17] AH Castro Neto, Francisco Guinea, Nuno MR Peres, Kostya S Novoselov, and Andre K Geim. The electronic properties of graphene. *Reviews of modern physics*, 81(1):109, 2009.

[18] Anna Orlof, Julius Ruseckas, and Igor V Zozoulenko. Effect of zigzag and armchair edges on the electronic transport in single-layer and bilayer graphene nanoribbons with defects. *Physical Review B*, 88(12):125409, 2013.

[19] PM Ostrovsky, IV Gornyi, and AD Mirlin. Theory of anomalous quantum hall effects in graphene. *Physical Review B*, 77(19):195430, 2008.

[20] R Rammal. Landau level spectrum of bloch electrons in a honeycomb lattice. *Journal de Physique*, 46(8):1345–1354, 1985.

[21] Javier D Sanchez-Yamagishi, Jason Y Luo, Andrea F Young, Benjamin M Hunt, Kenji Watanabe, Takashi Taniguchi, Raymond C Ashoori, and Pablo Jarillo-Herrero. Helical edge states and fractional quantum hall effect in a graphene electron–hole bilayer. *Nature nanotechnology*, 12(2):118, 2017.

[22] Yuhe Zhang, Ganesh Jaya Sreejith, Nathan D Gemelke, and Jainendra K Jain. Fractional angular momentum in cold-atom systems. *Physical review letters*, 113(16):160404, 2014.

[23] Yuhe Zhang, GJ Sreejith, and JK Jain. Creating and manipulating non-abelian anyons in cold atom systems using auxiliary bosons. *Physical Review B*, 92(7):075116, 2015.